Petroleum Science xxx (xxxx) xxx

Contents lists available at ScienceDirect

Petroleum Science

journal homepage: www.keaipublishing.com/en/journals/petroleum-science

Original Paper

# Effect of petroleum chemical fraction and residual oil content in saline lacustrine organic-rich shale: A case study from the Paleogene Dongpu Depression of North China

Chen-Xi Zhu [a, b], Fu-Jie Jiang [a, b, *], Peng-Yuan Zhang [c], Zhao Zhao [d], Xin Chen [e], Yu-Qi Wu [a, b], Yuan-Yuan Chen [a, b], Wei Wang [a, b], Ze-Zhang Song [a, b], Tao Hu [a, b], Tian-Wu Xu [f], Yong-Shui Zhou [f]

[a] State Key Laboratory of Petroleum Resources and Prospecting, China University of Petroleum (Beijing), Beijing, 102249, China
[b] Basin and Reservoir Research Center, China University of Petroleum (Beijing), Beijing, 102249, China
[c] Key Laboratory of Cenozoic Geology and Environment, Institute of Geology and Geophysics, Chinese Academy of Sciences, Beijing, 100191, China
[d] Tianjin Branch of CNOOC Ltd, Tianjin, 300459, China
[e] Shenzhen Branch, CNOOC China Limited, Shenzhen, Guangdong, 518000, China
[f] Zhongyuan Oilfield Branch, SINOPEC, Henan, 457001, China

ARTICLE INFO

*Article history:*
Received 19 January 2022
Received in revised form
16 June 2022
Accepted 15 September 2022
Available online xxx

Edited by Teng Zhu and Jia-Jia Fei

*Keywords:*
Oil fractionation
Residual oil
Saline lacustrine shale
The Dongpu Depression

ABSTRACT

Halite and gypsum minerals in saline shale make the retention mechanism and chemical fractionation of residual oil unique. The Dongpu Depression in North China is a typically saline lacustrine basin with developing halite and gypsum. The effect of gypsum minerals on residual oil content and chemical fractionation remains unclear. In this study, shale samples with different gypsum contents were used in organic geochemical experiments, showing that the high total organic matter (TOC) content and type II kerogen leads to a high residual oil content, as shown by high values of volatile hydrocarbon ($S_1$) and extractable organic matter (EOM). XRD and FE-SEM result indicate that the existence of gypsum in saline shale contributes to an enhanced pore space and a higher residual oil content in comparison to non-gypsum shale. Additionally, the increase in the gypsum mineral content leads to an increase in the saturated hydrocarbon percentage and a decrease in polar components percentage (resins and asphaltene). Furthermore, thermal simulation experiments on low-mature saline shale show that the percentage of saturated hydrocarbons in the residual oil is high and remains stable and that the storage space is mainly mesoporous (> 20 nm) in the oil expulsion stage. However, the saturated hydrocarbons percentage decreases rapidly, and oil exists in mesopores (> 20 nm and < 5 nm) in the gas expulsion stage. In general, gypsum is conducive to the development of pore space, the adsorption of hydrocarbons and the occurrence of saturated hydrocarbon, leading to large quantities of residual oil. The data in this paper should prove to be reliable for shale oil exploration in saline lacustrine basins.


## 1. Introduction

The transformation of international energy structure makes development and utilization of unconventional hydrocarbons resources to become the mainstream (Laughrey et al., 2009; Scarlat et al., 2015; Tan et al., 2015; Cen et al., 2016; Huang et al., 2020). The continuous development of the shale oil resources urges it become an important supporting part of the world's oil and gas resources, including Barnett shale (Jarvie, 2012; Han et al., 2015; Wang et al., 2022b), Bakken shale (Schmoker, 1996; Soeder, 2018) and Woodford shale in America (Cardott, 2012), and Duvernay shale in western Canada (Wang et al., 2017). Shale interbedded with evaporite, including chloride, sulfate and carbonate, in saline lacustrine basins has become important source rocks and reservoirs for unconventional oil and gas (Peters et al., 1996; Grice et al., 1998; Liang et al., 2017; Zou et al., 2019a, 2019b; Hu et al., 2021a; Zhu

* Corresponding author. State Key Laboratory of Petroleum Resources and Prospecting, China University of Petroleum (Beijing), Beijing, 102249, China.
*E-mail address:* jfjhtb@163.com (F.-J. Jiang).

https://doi.org/10.1016/j.petsci.2022.09.013


Please cite this article as: C.-X. Zhu, F.-J. Jiang, P.-Y. Zhang *et al.*, Effect of petroleum chemical fraction and residual oil content in saline lacustrine organic-rich shale: A case study from the Paleogene Dongpu Depression of North China, Petroleum Science, https://doi.org/10.1016/j.petsci.2022.09.013

et al., 2021; Wang et al., 2022a). Previous studies have shown that the paleoenvironment of saline lacustrine basins is conducive to the organic matter enrichment (Zhang and Yang, 1998; Zheng and Yang, 1999; Zhu et al., 2006; Grosjean et al., 2009; Wang et al., 2020b; Zhang et al., 2022c). Additionally, the saline shale has lower hydrocarbon generation threshold and higher hydrocarbon generation and expulsion capacity (Lewan and Ruble, 2002; Manzi et al., 2007; Jiang et al. 2016a, 2018, 2019; Zhang et al., 2021a).

The saline shale in lacustrine basins is widely distributed around the world, such as the Green River shale of Piceance Creek Basin (Tänavsuu-Milkeviciene and Frederick Sarg, 2012) and Uinta Basin in America, the Dongpu Depression (Huang et al., 2018; Guo and Jin, 2021), the Jiyang Depression (Zhang et al., 2016; He et al., 2018) and the Huanghua Depression (Qu et al., 2018; Zhang et al., 2020) of the Bohai Bay Basin in eastern China. The sedimentary environments of these areas have experienced dramatic variations from freshwater lake facies to high saline lake facies (Hackley and SanFilipo, 2016). Because of the frequently changing sedimentary environment, the distribution of shale is highly heterogeneous (López-Gamundí, 2010; Zou et al., 2012; Lin et al., 2013), which makes the fractionation and retention of oil in saline shale system more complex. The definition of shale oil is still ambiguous (Jarvie, 2012; Zou et al., 2012). Jarvie (2012) defined oil in mudstone or mud–sand interbedding as shale oil resource system. The liquid hydrocarbons preserved in mudstone or shale are considered as shale oil by Zou et al. (2012). In this paper, the oil stored in organic rich laminar mudstone or closely associated lithology, such as sandstone interbeds, is defined as shale oil (Zou et al., 2019a). Many studies have focused on the heterogeneity of shale distribution (Tang et al., 2018; Hu et al., 2021b), mineralogical composition (Li et al., 2019; Zhang et al., 2019a; Hafiz et al., 2020), occurrence space (Guan et al., 2020; Zhu et al., 2021) and shale oil–bearing properties (Su et al., 2019; Huang et al., 2020).

Previous studies have suggested that chemical fractionation occurs during the process of oil migration (Lafargue et al., 1990). The extracts of conventional sandstones and carbonate reservoirs have elevated saturates, while those of the source rocks are enriched in asphaltenes and resins which are also the results of the hydrocarbon expulsion fractionation (Brenneman and Smith, 1958; Tissot and Welte, 1984). Jarvie (2014) proposed that the oil migration over the distance of centimeters within source rocks leads to the chemical fractionation. Polar compounds have a large molecular size and high affinity with organic matter, which can seal low–permeability rocks (Leythaeuser and Schaefer, 1984; Wilhelms et al., 1990; Sandvik et al., 1992). Therefore, the oil components in shale oil system are not only closely associated with the oil recovery, but also affect the economic potential of exploration (Jarvie, 2015). The shale oil with developed lamina and higher organic matter content is easier to fractionate, and the light aromatic component are easier to migrate and form reservoirs (Zou et al., 2019a; Hu et al., 2020). In addition, clay minerals are also conducive to the retention of polar compounds in shale system (Han et al., 2015). However, due to the complex properties of saline shale (Li et al., 2021), the chemical fractionation of oil in shale system in saline lacustrine basins and its influence on retention mechanism are still ambiguous, which need to further studied. The Dongpu Depression, characterized by massive shale–gypsum interbedded rocks, is a typical saline lacustrine basin in the Bohai Bay Basin, eastern China (Wang et al., 2020c; Zhang et al., 2021a; Zhu et al., 2021), which is a candidate study target for saline shale. Therefore, based on the samples of the Dongpu Depression saline shale, this study aims: (1) to determine the content and properties of the retention oil; (2) to reveal the effects of organic matter and mineral contents (especially gypsum) on the chemical composition and the retention oil content of the saline shale system; (3) to analyze the occurrence space and chemical fractionation of the retention oil under different thermal maturities in saline shale.

## 2. Geological setting

In the early Cenozoic (~50–40 Ma) Himalayan movement, the eastern China gradually developed from the early North China craton basin to a rifting basin under the collision of the Pacific plate and the Indian Ocean plate, resulting in the gradual formation of the Bohai Bay Basin (Molnar and Tapponnier, 1975; Yin and Harrison, 2000; Jia et al., 2004). The Dongpu Depression, located in the southwest of the Bohai Bay Basin, is a typical lacustrine rifting basin, with an area of ~5300 $km^2$ (Chen et al., 2000; Wang et al., 2015; Lyu and Jiang, 2017). The Dongpu Depression has an NNE–trending and can be subdivided into Eastern Sag Belt, Central Uplift, Western Sag Belt and Western Slope Belt from east to west (Fig. 1) (Chen et al., 2013). The Paleogene sediments contains the Kongdian, Shahejie and Dongying Formations (Fig. 2) (Hou et al., 2001; Su et al., 2006; Qi and Yang, 2010). The Member 3 of the Eocene Shahejie Formation is further divided into three sub–members: upper, middle and lower formations based on the various stratigraphic subdivision schemes (Fig. 2) (Gao et al., 2011). The base ages of Member 3 are from 43.59 ± 0.57 Ma to 36.08 ± 0.57 Ma (Wang et al., 2020a). During the interval presented by the Member 3 of the Shahejie Formation extensive thick salt rock over 500 m deposited in the Dongpu Depression (Zhu et al., 2021), and the lower Member 3 of the Shahejie Formation, distributed in several sags with a depth of ~3000–5200 m, is the maincarrier of shale oil and is dominated by clastic shale and mudstones, carbonate rocks, and evaporites (Jiao et al., 2014; Shao et al., 2018a; Hu et al., 2022a, 2022b).

## 3. Samples and experiment

The 16 samples in this study were from 8 wells in the north region of Dongpu Depression (Fig. 1c), and all samples were from the lower Member 3 of the Shahejie Formation. The sedimentary environment of the selected wells was deep and semi–deep lake facies.

### 3.1. Rock–Eval pyrolysis and total organic carbon content determination

A total of 16 samples were pulverized to 100 mesh in preparation for the experiments of pyrolysis and the total organic carbon content (TOC). The hydrochloric acid solution (12.5%) was added to the powder samples to remove the inorganic carbon. The test started after washing the acidic solution in the sample with distilled water. The TOC content was determined using LECO CS–230 analyzer, and the Rock–Eval pyrolysis was performed using a Rock–Eval II instrument (Espitalié et al., 1977). The volatile hydrocarbon ($S_1$) was obtained when the temperature reached 300 °C, and the pyrolyzed hydrocarbon ($S_2$) and the temperature of maximum hydrocarbon generation ($T_{max}$) were obtained when the temperature reached 300–600 °C.

### 3.2. X–ray diffraction and scanning electron microscopy

The mineralogical composition was obtained by a TTR–III X–ray diffractometer. 16 powder samples with particle size less than 10 μm were extracted by using the centrifugal separation method to determine the relatively mineral content, and the samples with particle size less than 2 μm were used for the determination of the clay content. The energy dispersive spectroscopy (EDS) was applied for determining the minerals composition. The thin sections of

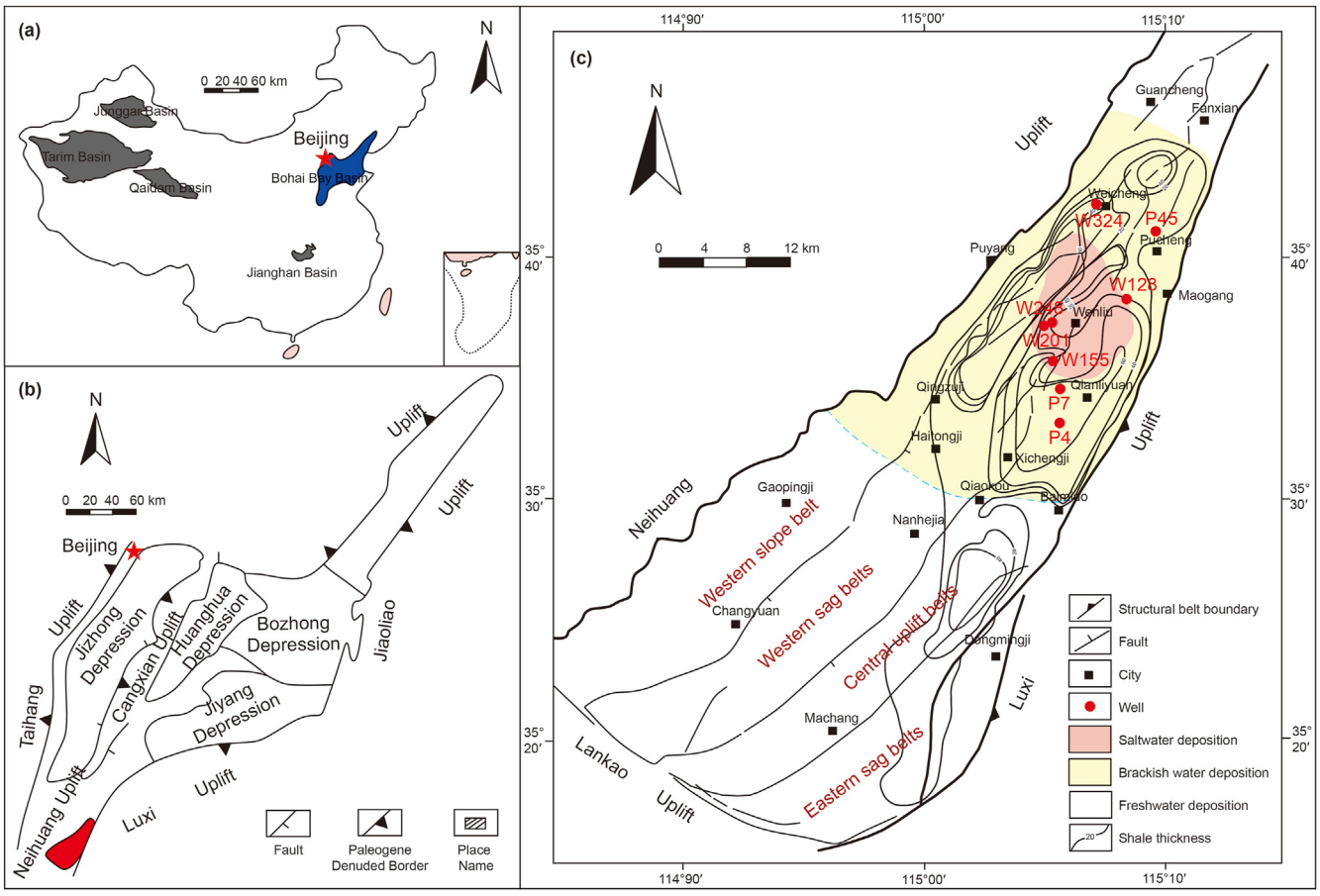


**Fig. 1.** Sketch map showing (**a**) the Bohai Bay Basin in China mainland are in the blue position; (**b**) the Dongpu Depression in the Bohai Bay Basin are in the red position; (**c**) the tectonic units, the shale thickness and the depositional environments of the Dongpu Depression. The location of cored wells in the study are annotated by red point (modified after Hao et al., 2007; Li et al., 2020a; Zhu et al., 2021).

samples with Au/Pd coating were identified by the scanning electron microscopy (Eseme et al., 2007).

### 3.3. Solvent extraction and fractionation

16 powder samples (100 mesh) and 5 samples after thermal simulation experiments were used for the solvent extraction and fractionation. The chloroform was added to samples, and the temperature was maintained at 70 °C in Soxhlet extractor for 48 h. Then, metallic copper was added to the mixture to remove natural sulfur. The collected extracts were separated into maltenes (organic solvent soluble components) and asphaltenes using hexane (Theuerkorn et al., 2008). Saturated hydrocarbons, aromatics hydrocarbon and polar components were separated by the column chromatography (based on $SiO_2$ and $Al_2O_3$) using a 2:1 mixture of dichloromethane (DCM) and *n*-hexane, and a 2:1 mixture of DCM and methanol, respectively (Radke et al., 1980).

### 3.4. Closed–system pyrolysis experiment

The sample with a high TOC content and a low maturity was selected as for the thermal simulation experiments, which is the most appropriate pyrolysis method to simulate petroleum retention and expulsion (Spigolon et al., 2015). The sample (30 g) crushing to 5–8 mm size and distilled water was put into the vacuum closed system. The closed system was filled with nitrogen gas and checked for leaks 3–5 times. The experiments were conducted at 18 °C, and the pyrolysis temperatures were set at 320 °C, 340 °C, 360 °C, 380 °C and 400 °C, respectively (Lewan et al., 2014). The heating rate was 1 °C/min, and temperature was held for 48 h after reaching the pyrolysis temperature using autoclave. The pyrolysis temperatures of 320–400 °C can be shown as the oil window (Lewan, 1985). The temperature error was less than 1 °C, and the pressure error was less than 0.1 MPa. After thermal simulation experiments, dichloromethane solution was used to flush the interior of the autoclave device and the oil discharge pipeline to obtain the discharged oil. Then, the sample was extracted to determine the residual oil content. The sum of the discharged oil content and the residual oil content is the oil generation (Wu et al., 2018). The ratio of oil generation content, gas generation content and oil retention content to sample mass is considered as the yield (Song et al., 2020).

### 3.5. $N_2$ adsorption experiment

5 samples after thermal simulation experiments (100 mesh) were at 110 °C for 24 h to remove water and residual gas in shale. The nitrogen adsorption-desorption isotherms were obtained at the pressure ranging from 0.001 to 0.990 under the condition of 77.3 K (−196 °C) liquid nitrogen. The Brunauer–Emmett–Teller (BET) (Rouquerol et al., 2007; Thommes et al., 2015) and the Barrett, Johner and Halenda (BJH) models (Barrett et al., 1951) were used to calculate the pore surface areas, the total pore volume and the average pore width.

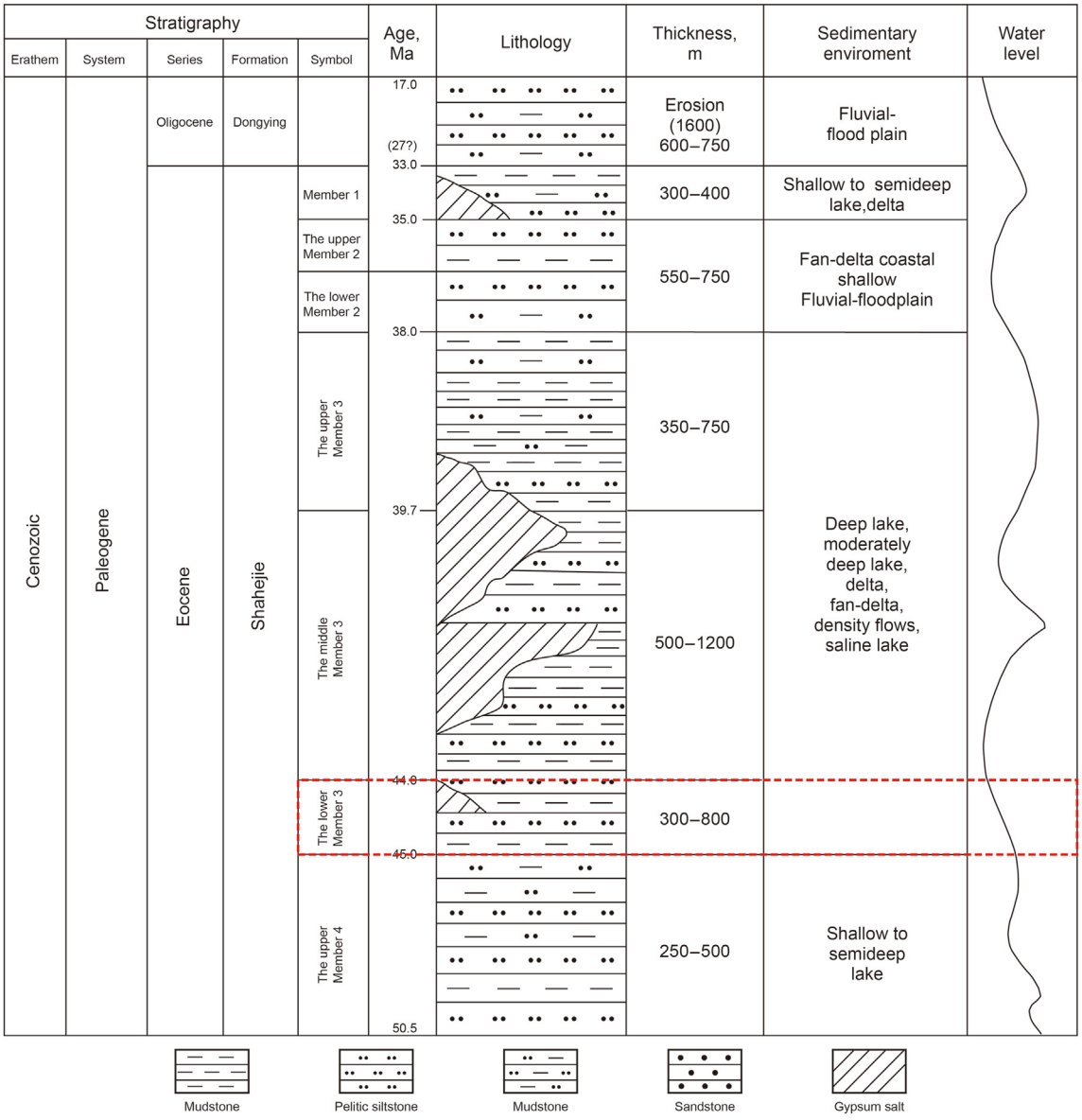


**Fig. 2.** Information of stratigraphy, depositional system of the Dongpu Depression. The strata for this study are annotated by a red rectangle in the lithology column. The typical pictures of cores are coming from the study strata (Wang et al., 2020a; Hu et al. 2021).

## 4. Result

### 4.1. Petrology and mineral compositions

The main minerals of the lower Member 3 of the Shahejie Formation shale are quartz (mean: 18.01%), calcite (mean: 32.03%) and clay (mean: 27.49%). The carbonate mineral content, ranging from 9.4% to 72.9% (mean: 42.5%), is the highest mineral and varies frequently (Fig. 3). The clay mineral content (12.1%–52.8%, mean: 27.49%) also occupies a dominant position and increases with the increasing depth. Pyrite deposited in the lower Member 3 of the Shahejie Formation, especially in ~3500–4200 m, and its content increases to 8.8% with the increasing depth (Fig. 4). One obvious characteristic is that evaporite minerals (gypsum and halite) account for a significant proportion. The halite content is 2.8% in the depth of 3697.21 m, while the gypsum is distributed in all the shale samples. The gypsum contents range from 0.20% to 13.3% (mean: 4.83%), and reaches the highest in ~3000–4000 m (Fig. 3).

Since the halite content in the samples is very small, our focus is on the gypsum minerals in evaporite. The quartz content is widely distributed when the gypsum content in shale is less than 5%, the maximum can be reached 31.3% and the minimum is 6.1%. But the quartz content is stably distributed between 16.9% and 22.5% when the gypsum content is greater than 5%, and the mean value is 19.77%. Additionally, the clay contents have the characteristics of wide distribution and overall downward trend, ranging from 12.1% to 52.8%, when gypsum content less than 5%. When the gypsum content larger than 5%, the clay content is ranging from 23.7% to 37% with an average of 28.4%.

### 4.2. Organic geochemistry

The TOC content ranges from 0.15% to 2.96% (mean: 1.18%), and the hydrocarbon generation potential (Pg) is 0.09–21.07 mg/g (mean: 5.37 mg/g). The maximum temperature of pyrolysis yield ($T_{max}$) is 422–597 °C (Sample a is 573 °C in the depth of 5001.7 m;

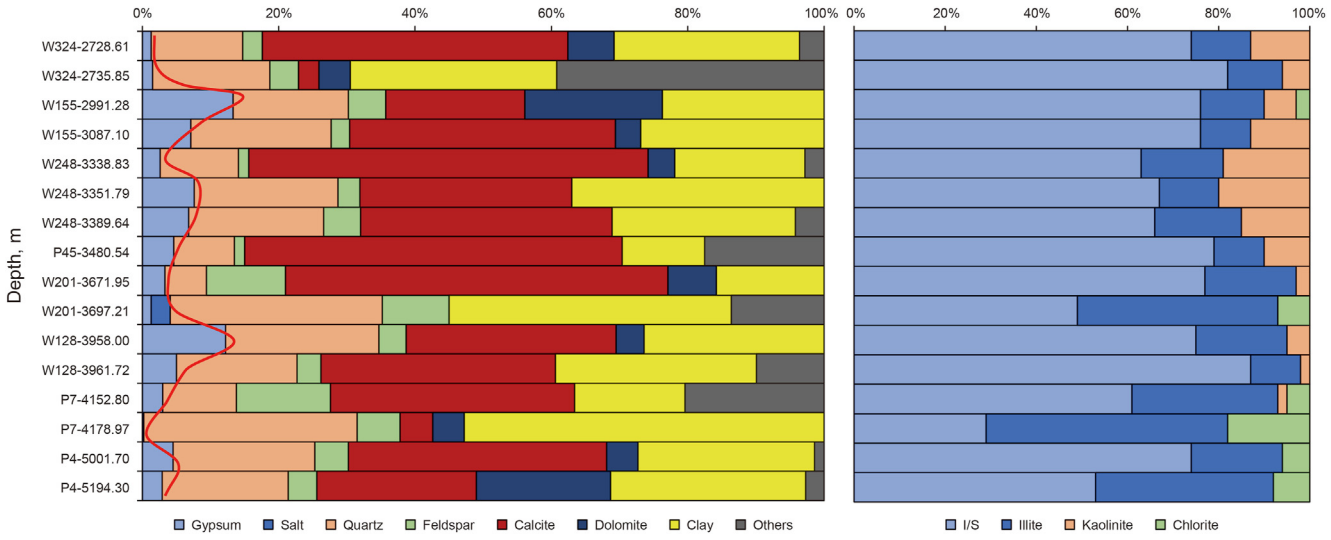


**Fig. 3.** Mineralogy of saline shale in the Dongpu Depression. The variation trend of salt rocks is annotated by a red curve.

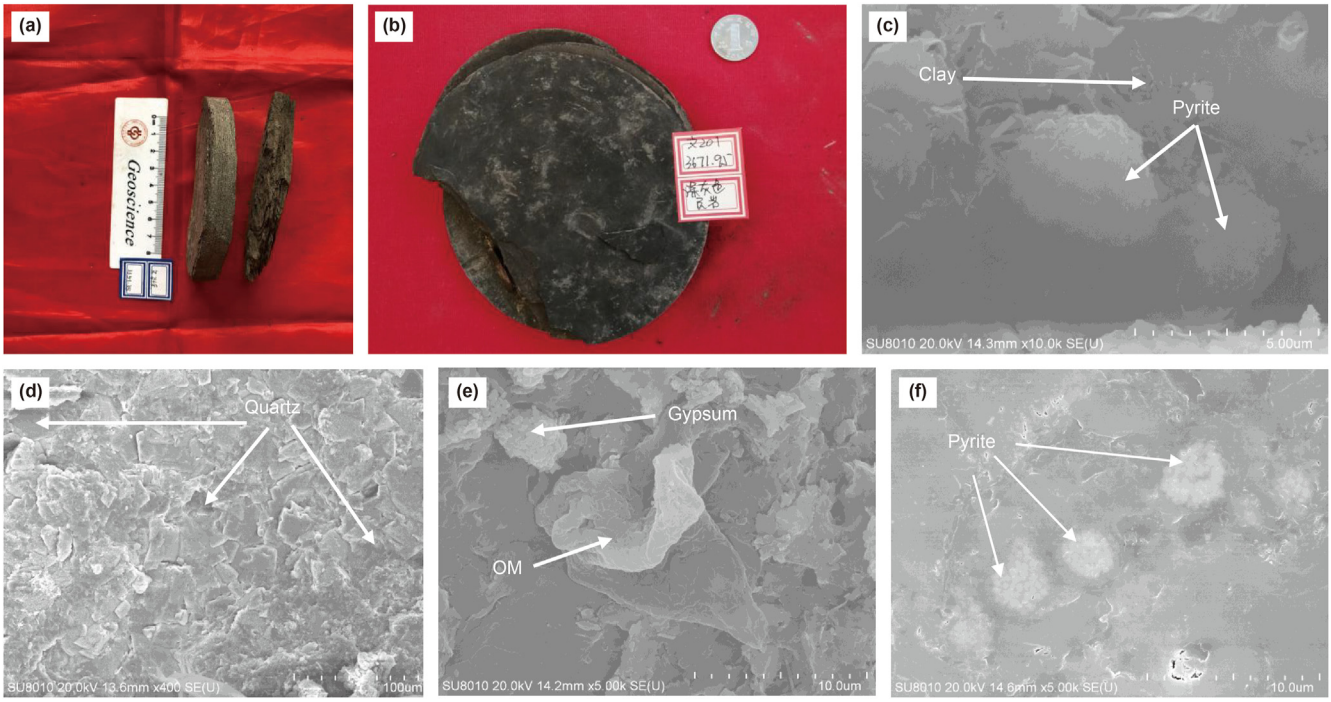


**Fig. 4.** FE-SEM images shows the typically petrological characteristics of saline shale in the Dongpu Depression. (**a**) Well W248, 3351.35 m, laminated shale; (**b**) Well W201, 3671.95 m, black organic-rich shale; (**c**) Well P7, 4178.97 m, Clay and framboidal pyrite development; (**d**) Well W201, 3687.21 m, Quartz development; (**e**) and (**f**) Well W155, 2991.28, Framboidal pyrite, gypsum and OM development.

Sample b is 597 °C in the depth of 5194.3 m), and the average of $T_{max}$ value after removing Samples a and b is 438 °C. The cross–plot of the hydrocarbon index (HI: $S_2$/TOC × 100, mg HC/g TOC) versus $T_{max}$ shows that the organic matter type of the lower Member 3 of the Shahejie Formation shale is dominated by type $II_1$ and $II_2$ kerogen and followed by type III kerogen. According to the TOC contents and organic matter type, samples are divided into three categories (Fig. 5):

Type A shale has the organic matter of type $II_1$ kerogen, and high TOC contents (1.08–2.96%) and Pg contents (5.75–21.07 mg/g); type B shale has the organic matter of type $II_2$ kerogen, and moderate TOC contents (0.63%–1.81%) and Pg contents (2.95–10 mg/g); type C shale has the organic matter of type III kerogen, and low TOC contents (0.15%–0.77%) and Pg contents (0.09–1.6 mg/g). Samples a and b cannot determine their organic matter type through $T_{max}$ value owing to the deeper burial depth and the higher maturity, but they are classified as type C shale due to their low Pg contents (Table 1).

In Fig. 6, the four black samples cannot be classified because of the high $T_{max}$. Excluding the four black samples buried at a depth of more than 5000 m, the saturated hydrocarbon percentage in raw samples, ranging from 5.41% to 77.06% (mean: 44.78%), gradually increases and then decreases with the increasing depth, while the aromatics percentage, ranging from 5.58% to 28.57%, decreases

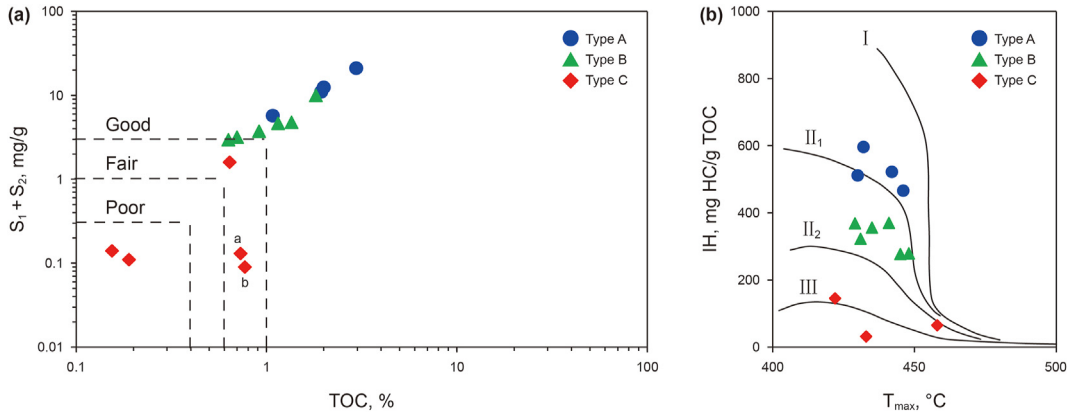


**Fig. 5.** (**a**) The pyrolysis $S_1$+$S_2$ versus the total organic matter (TOC) of the lower Member 3 of the Shahejie Formation shale in the Dongpu Depression, showing the generative source rock potential and (**b**) the hydrocarbon index (HI) versus the pyrosis $T_{max}$ of the lower Member 3 of the Shahejie Formation shale in the Dongpu Depression, showing the kerogen type.

**Table 1**
Geochemical characteristics of original shale samples.

| | Well | Depth, m | TOC, % | $S_1$, mg/g | $S_2$, mg/g | $T_{max}$, °C | EOM, mg/g |
|---|---|---|---|---|---|---|---|
| Type A | W155 | 3087.1 | 1.08 | 0.72 | 5.03 | 446 | 3.119873 |
| | **W155** | **2991.28** | **1.94** | **1.14** | **9.92** | **430** | **4.86538** |
| | W324 | 2735.85 | 1.998 | 0.57 | 11.91 | 432 | 2.444685 |
| | W248 | 3351.79 | 2.962 | 5.61 | 15.46 | 442 | 11.42373 |
| Type B | W201 | 3671.95 | 1.352 | 1.04 | 3.75 | 445 | 1.625 |
| | P45 | 3480.54 | 0.7 | 0.59 | 2.59 | 441 | 2.86068 |
| | W248 | 3389.64 | 1.814 | 3.31 | 6.69 | 429 | 5.929412 |
| | W248 | 3338.83 | 0.6297 | 0.92 | 2.03 | 431 | 2.959514 |
| | W324 | 2728.61 | 0.9138 | 0.5 | 3.25 | 435 | 2.552894 |
| | W128 | 3961.72 | 1.15 | 1.43 | 3.21 | 448 | 4.069341 |
| Type C | P4 | 5194.3 | 0.77 | 0.04 | 0.05 | 597 | 0.117794 |
| | P4 | 5001.7 | 0.73 | 0.02 | 0.11 | 573 | 0.08957 |
| | P7 | 4178.97 | 0.1893 | 0.05 | 0.06 | 433 | 0.276805 |
| | W128 | 3958 | 0.64 | 0.67 | 0.93 | 422 | 2.069743 |
| | W201 | 3697.21 | 0.1542 | 0.04 | 0.1 | 458 | 0.271605 |

Note: Bolded sample was selected for the thermal simulation experiment.

tardily and then keep stable with the increasing depth. The percentage of polar components (resins and asphaltenes) gradually decreases from 8.24% to 62.90% with an average of 29.39%. When the depth exceeds 4000 m, the polar components percentage gradually increases. It should be noted that the $S_1$ content of samples ranging from 0.01 to 0.02 mg/g on type C shale, there may be experimental errors in saturated hydrocarbon percentage in raw samples due to low residual oil content, which needed to further discuss in the future.

### 4.3. Thermal simulation experiments

Easy%$R_o$ can be determined by the kinetic model (Sweeney and Burnham, 1990), and the value with increasing pyrolysis temperature of the post-pyrolysis shale are presented in Table 2. With the increasing temperature, the residual oil yield decreases from 3.31 mg/g to 0.81 mg/g. The oil expulsion yield gradually increases to 2.01 mg/g before 360 °C and then starts to decrease. The residual oil yield follows a downward trend from 3.43 mg/g to 0.84 mg/g. The oil generation yield remains stable at ~3.5–4.12 mg/g before 360 °C, with an average value of 3.80 mg/g, and then decreases. The gas expulsion yields increases continuously from 0.17 mL/g to 4.78 mL/g before 360 °C, and drops to 2.60 mL/g in 380 °C, and then increases rapidly to 10.16 mL/g.

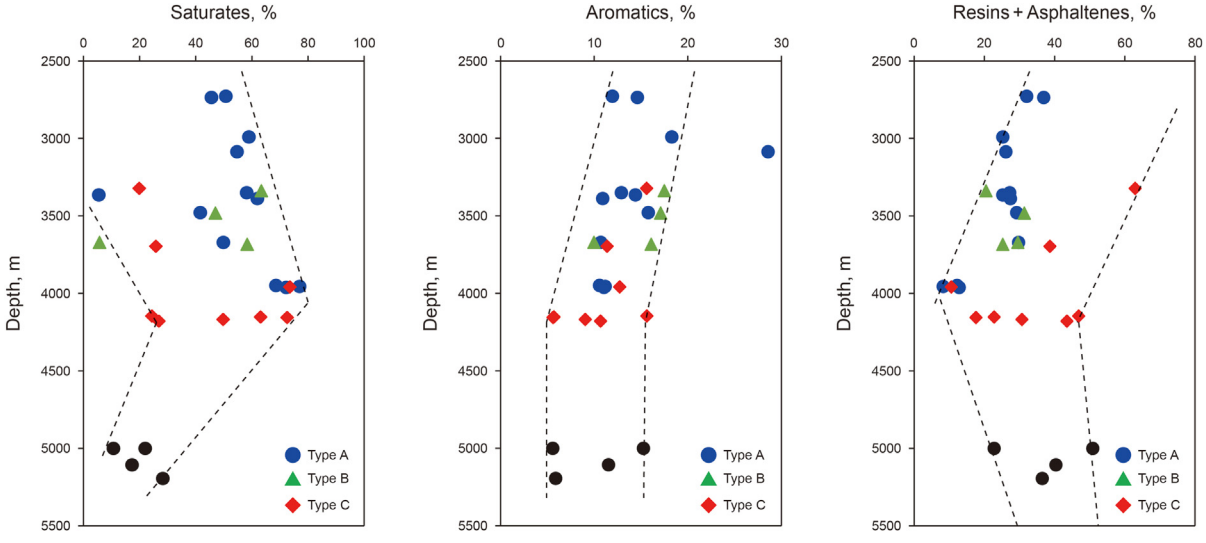


**Fig. 6.** Graph showing the chemical composition of residual hydrocarbon.

**Table 2**
Generation, expulsion and retention oil production and retention oil component content.

| Temperature, °C | Easy$R_o$, % | Oil expulsion, mg/g | Oil retention, mg/g | Oil generation, mg/g | Gas Expulsion, mL/g | Chemical component content of retained oil | | |
|---|---|---|---|---|---|---|---|---|
| | | | | | | Saturates, % | Aromatics, % | Resins + Asphaltenes, % |
| 320 | 0.81 | 0.66 | 3.44 | 4.12 | 0.17 | 32.54 | 19.82 | 36.98 |
| 340 | 0.98 | 1.05 | 2.43 | 3.50 | 4.10 | 34.18 | 21.52 | 27.43 |
| 360 | 1.21 | 2.01 | 1.73 | 3.79 | 4.78 | 33.33 | 27.59 | 25.86 |
| 380 | 1.84 | 0.25 | 0.99 | 1.25 | 2.60 | 22.55 | 34.31 | 34.31 |
| 400 | 2.17 | 0.47 | 0.84 | 1.32 | 10.16 | 12.20 | 21.95 | 26.83 |

## 5. Discussion

### 5.1. Factors controlling the residual oil content

#### 5.1.1. Residual oil in saline shale

The gypsum–halite rocks mainly deposited in the deep and semi–deep lake facies in the northern area of the Dongpu Depression (Zhu et al., 2021) which the shale mainly deposited. The abundance of organic matter can be determined by the TOC content and the Pg content (Peters, 1986; Tissot and Welte, 1984). According to the evaluation criteria of lacustrine source rocks, shale can be divided into four categories: non (TOC < 0.4%; Pg < 0.5 mg/g); poor (0.4% < TOC < 0.6%; 0.5 mg/g < Pg < 2 mg/g); fair (0.6% < TOC < 1%; 2 mg/g < Pg < 6 mg/g); good (TOC > 1%; Pg > 6 mg/g) (Huang et al., 1984; Chen et al., 1997; Jia et al., 2016). Type A and B shale are fair–good source rocks and have type II kerogen, indicating that they have the high organic matter content and the high hydrocarbon generation potential. The hydrocarbon generation parent material of type II kerogen mainly derives from the mixture of plankton and microorganisms (Zhang, 1992). Type C shale is fair and no source rocks, with the low organic matter content and hydrocarbon generation potential (Fig. 5). The hydrocarbon generation parent material is mainly terrestrial higher plants (Zhang, 1992). The saline shale of Jianghan Basin (Qianjiang Formation) and Qaidam Basin (Dameigou Formation) are also mainly type II kerogen sourced from the aquatic organisms in lakes (Hou et al., 2017; Wang et al., 2021). The TOC contents of these basins are 1.0%–10% (mean: 1.2%) and 0.6%–10.7% (mean: 3.83%), respectively (Wang et al., 2019b). Additionally, these lacustrine basins also have high $S_1$ content, mostly greater than 1 mg/g (Hou et al., 2017), showing the potential of the saline lacustrine shale. In summary, the saline lacustrine shale has high TOC content with developing type II kerogen of organic matter.

#### 5.1.2. Effect of the TOC

The light hydrocarbons ($C_{1-4}$) that remain in shale will gradually volatilize during coring process (Zhu et al., 2015), and massive loss of light hydrocarbons ($C_{6-14}$) will also occur in the processes of the sample preparation and solvent evaporation separation of extract during the experiments of obtaining EOM (Bordenave, 1993). In addition, when the temperature is less than 300 °C, the content of residual hydrocarbons (free hydrocarbons) in the rock is the obtained $S_1$ value in the pyrolysis experiments, while the high–carbon–number hydrocarbons and NSO compounds with a boiling point higher than 300 °C in the sample will be ignored (Vankreve, 1965). Therefore, $S_1$ and EOM contents can only be used as a part of measuring the content of residual oil (Cooles et al., 1986). The light hydrocarbon recovery coefficients at different evolution stages in Jiyang Depression, which is adjacent to Dongpu Depression, were selected to restore the light hydrocarbon of $S_1$ and EOM in this study (Zhu et al., 2015). The correlation between the restored value and TOC content is consistent with the correlation between the measured value and TOC content (Fig. 7). Thus, the following analysis still uses measured values.

The extractable organic matter (EOM) and $S_1$ values can represent the residual oil content (Jarvie, 2012), which have a positive correlation with the TOC content (Fig. 7a). With the increase in the TOC content, the residual oil content of type A and B shale increases rapidly (Fig. 7a). The correlation between the residual oil and TOC content of type A shale is the best, and the coefficient of determination ($R^2$) is 0.7. Whereas the residual oil content of type C shale show a slow upward trend with the increasing TOC content and their $R^2$ is only 0.05. For type B shale, it is found that the coefficient of determination between EOM value and TOC content is 0.18, while the correlation coefficient between $S_1$ and TOC content is 0.7 (Fig. 7b). The reason is that EOM contains some coke asphalt, while $S_1$ does not (Vankreve, 1965), thus the correlation between EOM value and TOC content is low. Sandvik and Pepper propoesed that ~10 g petroleum can retained per 100 g TOC or 100 mg/gTOC in organic matter (Pepper, 1991; Sandvik et al., 1992). The TOC content has an obvious positive correlation with $S_1$ and EOM (Fig. 7), indicating that TOC is one of the key factors controlling the residual oil content in the shale system (Pang et al., 2018; Zhang et al., 2019b).

#### 5.1.3. Effect of the maturity

The organic matter maturity of shale also can affect the residual oil content (Jarvie et al., 2007). The $S_1$ values of samples a and b are 0.02 mg/g and 0.04 mg/g respectively, and the $T_{max}$ values are 597 °C and 573 °C, indicating that they are in the over mature stage (Fig. 8). Because the too high maturity can affect the real result (Luo et al., 2011), samples a and b are excluded from Fig. 8. The shale of the lower Member 3 of the Shahejie Formation is in the mature stage, which is the main oil generation stage (Fig. 8). The residual oil content gradually decreases after reaching the maximum temperature at this stage. Variations of the maturity can lead to the expansion of the kerogen structure, which affects the fractionation and retention of petroleum in organic rich shale (Larsen and Li, 1997; Ertas et al., 2006; Kelemen et al., 2006). The similar that the highest oil content occurs in shale when the $T_{max}$ value is 445 °C is consisted with that presented in the Mississippian Barnett shale (Texas) and the Toarcian Posidonia shale (Lower Saxony, Germany) (Han et al., 2017).

#### 5.1.4. Effect of the clay mineral

The low $R^2$ value (< 0.2) indicates the correlation between clay mineral content and residual oil content is weak. However, type A shale shows a good positive correlation between the residual oil content and the clay minerals content, which result from the high residual oil content of sample c (Fig. 9a and b). It can be inferred that sample c is affected by high organic matter content (Fig. 7). The adsorption capacity of minerals to hydrocarbons is weaker than that of organic matter (Jarvie, 2012; Sang et al., 2018). However, many inorganic characteristics, such as mineral composition, porosity, permeability, fracture and cementation, can also control oil and gas retention (Han et al., 2015). The adsorption capacity of clay minerals to hydrocarbons is greater than that of clastic

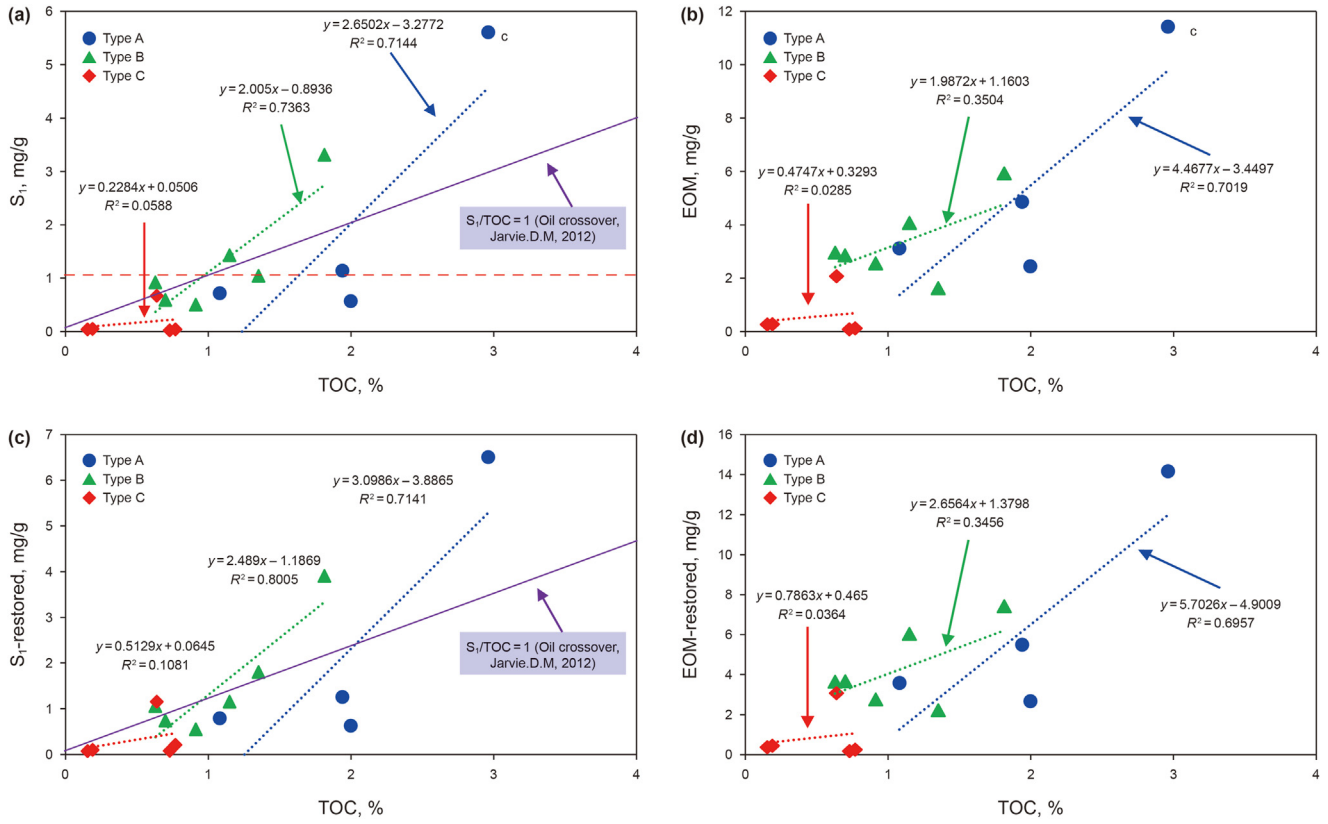


**Fig. 7.** Graphs showing the effect of TOC on $S_1$ and EOM yield of shale from type A, B and C in the Dongpu Depression. (**a**) The significant relationship demonstrates the major effect of TOC on $S_1$ yield from type A and B; (**b**) the major effect of TOC on EOM yield from type A. EOM represents the extraction organic matter; (**c**) and (**d**) the effect of TOC on restored $S_1$ and EOM yield.

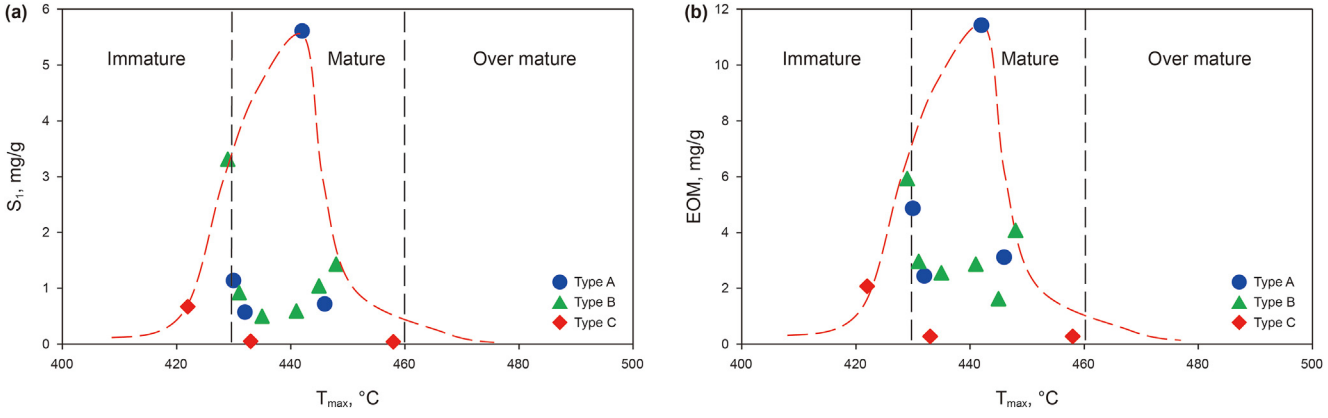


**Fig. 8.** The effect of organic matter maturity on $S_1$ and EOM yield of shale in the Dongpu Depression. (**a**) The effect of pyrolysis $T_{max}$ on $S_1$ yield. (**b**) The effect of pyrolysis $T_{max}$ on EOM yield. The red curve represents the variation trend.

minerals such as quartz and carbonate (Li et al., 2016), which can be attributed to the fact that the unique surface area of clay minerals is significantly larger than that of brittle minerals and can increase the adsorption area for hydrocarbons (Wang et al., 2016). Nevertheless, the high adsorption capacity of clay minerals to petroleum can also reduce the reservoir porosity and permeability, resulting in the low fluidity of shale oil (Ning et al., 2020). In the present study, the clay mineral contents of most samples are less than 30% and have a weak influence on the residual oil content (Fig. 9a and b). Huang et al. (2018 and b) suggested that the increase of clay content in shale from the Dongpu Depression corresponds to the decrease of residual oil content (Huang et al., 2018a; 2018b). Chen et al. (2020) believed that the clay mineral content which is more than 30% is negatively correlated with the residual oil content in shale of Ordos Basin.

### 5.1.5. *Effect of the brittle minerals*

Since there are too few samples in the downward trend, referring to Shao et al. (2018) research data on saline shale in Dongpu Depression, it shows that quartz and gypsum and residual oil content increase first and then decrease. Before the quartz content reaches 21.1%, the residual oil content increases with the increase of

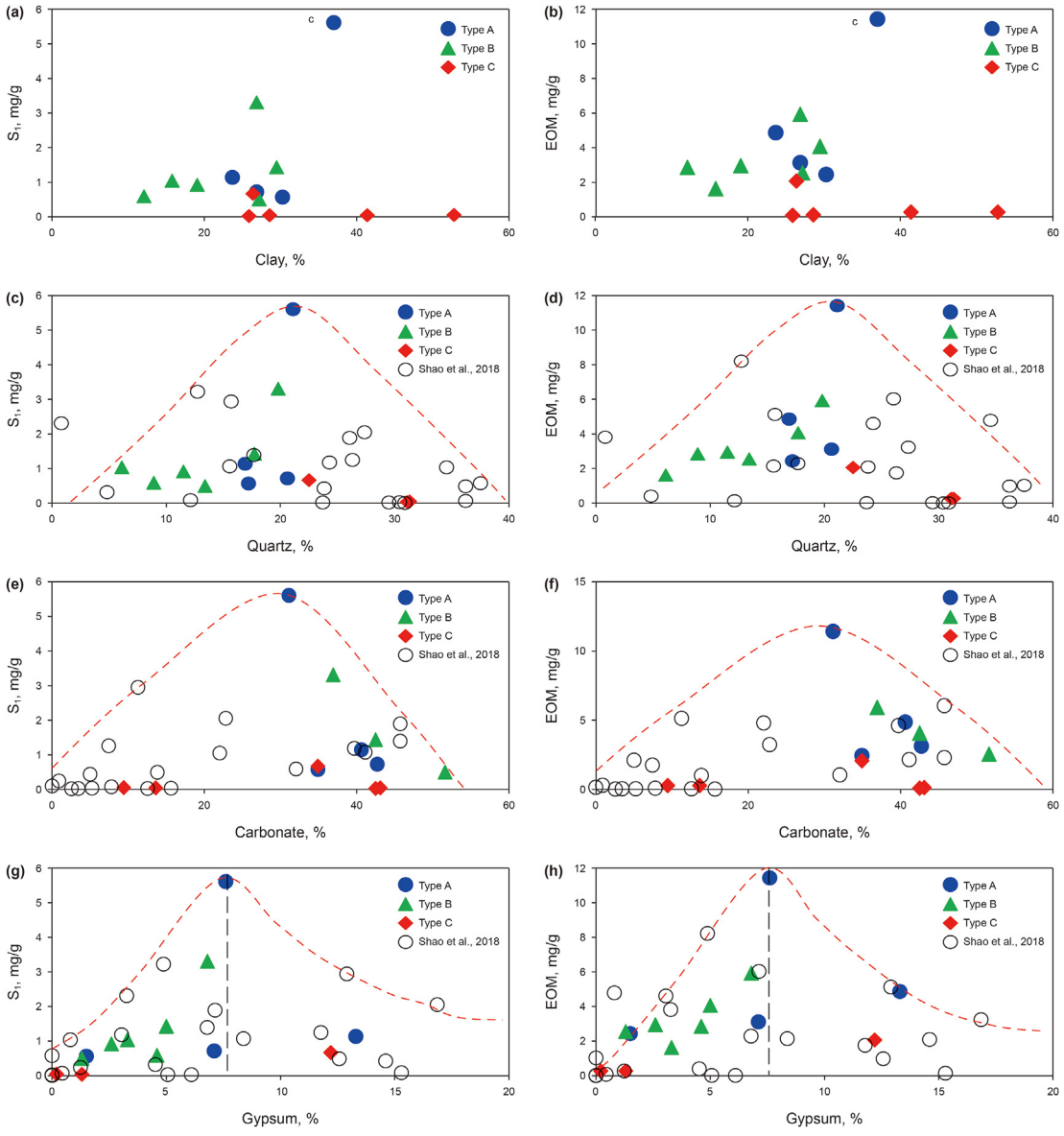


**Fig. 9.** The effect of clay, quartz and gypsum on $S_1$ and EOM yield of shale in the Dongpu Depression. (**a**) The effect of the clay mineral content on $S_1$ yield; (**b**) the effect of the clay mineral content on EOM yield; (**c**) the effect of the quartz mineral content on $S_1$ yield; (**d**) the effect of the quartz mineral content on EOM yield; (**e**) the effect of the carbonate mineral content on $S_1$ yield; (**f**) the effect of the carbonate mineral content on EOM yield; (**g**) the effect of the gypsum mineral content on $S_1$ yield; (**h**) the effect of the gypsum mineral content on EOM yield. The black circles in (**c**), (**d**), (**e**), (**f**), (**g**) and (**h**) is quoted from Shao et al., (2018).

quartz content, which can be attributed to the fact that quartz can provide support for pores, and can further block out diagenesis and maintain high liquid hydrocarbon storage capacity of shale (Yang et al., 2018). The organic acids produced during the kerogen decomposition can migrate during hydrocarbons generation, resulting in the corrosion of quartz and feldspar minerals (Bjørlykke, 1997, 1998; Nygård et al., 2004; Oelkers et al., 1996; Mondol et al., 2007), and the corroded space can further provide intraparticle pores for residual oil. In addition, the existence of evaporite minerals indicates that the bottom water was a relatively reducing environment, in which quartz cementation can occur (Emmings et al., 2019, 2020), which can inhibit the compaction of mudstone (Fishman et al., 2015; Milliken and Olson, 2017) and provide storage space for oil occurrence (Fig. 9c and d).

On the other hands, the residual oil content decreases rapidly after the quartz content exceeding 21.1%. Although quartz can still provide the storage space for residual oil, the synchronous occurrence of high contents of clay mineral (mean: 40.2%) may reduce the storage space (Fig. 9e and f) (Chen et al., 2020). If the clay mineral content is too high, the mixed layer of illite and montmorillonite can be transformed into illite at ~60–100 °C ($R_o$ ~0.8%) during diagenesis (Merriman, 1999; van de Kamp, 2008; Peltonen et al., 2009). Montmorillonite can release a large amount of silica and form smaller and harder micro quartz during the process of transformation to illite, which fills large number of pores (van de Kamp, 2008; Thyberg et al., 2010). These processes can further affect the physical properties of mudstone and reduce the storage space of residual oil (Lindgreen et al., 1991; Bjørlykke, 1998). The transformation from montmorillonite to illite of samples occurred at ~2500–4000 m ($R_o$ ~0.8%–1.2%) (Fig. 3), which contributed to the formation of micro quartz and reduction of the storage space for residual oil (Shou and Yuan, 1990; Zhao et al., 1992; Sun, 1996).

Additionally, the TOC contents of samples with quartz content of more than 21.5% are less than 0.65%, and these samples have a weaker adsorption capacity of organic matter (Fig. 7). The effect of carbonate minerals, as another brittle mineral, on the content of residual oil has the same trend as that of quartz (Fig. 7e and f). Carbonate minerals are not only easily dissolved to form intergranular or intra-granular dissolved pores and easily recrystallized to form inter-granular pores (Jiang et al., 2016b). The higher content of brittle minerals such as quartz and carbonate can result formation of natural fractures which is easy to form complex fractures and achieve the extension and connection of fracture networks. The developed microfractures would promote the oil loss in the shale system and then result in the decreasing oil enrichment (Rodriguez and Philp, 2010).

Gypsum ($CaSO_4$), found to be usually interbedded with organic rich source rocks, is a typical evaporite mineral in saline lacustrine basins (Valyashko, 1963; Huang et al., 2003; Jiang et al., 2004; Jin et al., 2008). The saline lakes generally distributed in arid regions with sensitive climate (Torgersen et al., 1986; Wang et al., 2002). Although, it is still controversial whether the sedimentary environment of the lake water is deep or shallow water during gypsum deposition process (Gao et al., 2011). It can be determined that it has been frequently diluted and concentrated (Anderson, 1977), and finally forms the interbedded deposition with organic-rich shale. The residual oil content gradually increases with the increasing gypsum content (Fig. 9g and h), which is due to the fact that large number of prosperous halophilic algae can be as hydrocarbon generating parent materials in the brackish–saline environments, and the organic rich sediments can also provide hydrocarbon basis for residual oil (Song et al., 2019; Hu et al. 2021). Actually, previous studies have found that the $S_1$ and EOM values of Qingshankou Formation shale in Songliao basin (freshwater–brackish water lacustrine basin) are 0.1 mg/g–7.0 mg/g (mean value: 1.1 mg/g) and 0.01–1.1% (mean value: 0.34%), respectively (Tang et al., 2014). The $S_1$ and EOM values of Chang 7 shale in Ordos Basin (freshwater–brackish water lacustrine basin) are 1.24–7.41 mg/g (mean value: 3.03 mg/g) and 0.24%–1.56% (mean value: 0.66%), respectively (Liu et al., 2017; Zhang et al., 2021b). But in the saline lacustrine basin, the $S_1$ value of Qianjiang Formation in Jianghan Basin is 0.17–21.2 mg/g (mean value: 5.02 mg/g) (Hou et al., 2017). Additionally, the inherent wettability of surface at the nanoscale also controls the petroleum migration in nanosized channels (Salehi et al., 2008; Xue et al., 2015). Gypsum, as a super hydrophilic mineral, is preferentially wetted by water at the scale, which can hinder the migration of oil in shale system and increase the retained oil content (Chang et al., 2018). The retained oil content begins to decrease after the gypsum content exceeding 7.5% (Fig. 10a, b and c), which may result from the formation of fracture pores during tectonic activities, further facilitating the interlayer migration of shale oil (Wang et al., 2017).

### 5.2. Fractionation of the residual oil

According to the chromatographic fractionation effect based on the polarity of petroleum components (Leythaeuser et al., 1987), the component fractionation of petroleum usually occurs during the initial migration and discharge of oil in shale. The preferential discharge sequence of hydrocarbon chemical components in petroleum is aliphatic, aromatic, resins and asphaltenes (Leythaeuser et al., 1987; Sandvik et al., 1992). The saturated hydrocarbon percentage in raw samples increases with the increase of the residual oil content (Fig. 11a and b). The saturated hydrocarbon percentage in raw samples tends to be stable and has a slight downward trend when the $S_1$ exceeds 1 mg/g, while its still remain high values of > 50% (Fig. 11a and b).

As shown in Fig. 6, the OSI values of samples with $S_1$ contents exceeding 1 mg/g are greater than 1, which indicates that the petroleum in the shale system is industrial movable oil, further implying that the residual oil contains both free oil and adsorbed oil (Bao et al., 2016; Gorynski et al., 2019). However, the free oil generally exists in intergranular pores and has a high saturated hydrocarbon percentage in raw samples (Wang et al., 2019a). Thus, it is considered that type A and B shale have high free oil content and are better exploration target for shale oil. The change of aromatic hydrocarbon percentage in raw samples, ranging from 5.69% to 28.57% (average 13.37%), is not obvious, and the influence of other factors on the aromatic hydrocarbon percentage in raw samples is weak (Fig. 11c and d). Although there may be experimental errors in the chemical component percentage of residual oil in type C shale, it does not affect the overall trend of saturated hydrocarbon and polar components percentage in raw samples.

Although the influences of TOC content and clay minerals on saturated hydrocarbons are not significant (Fig. 12a and b), the organic matter content of type A and B shale has a significant influence on aromatic hydrocarbons and polar components percentage (Fig. 12d and g). The selective adsorption of petroleum components on clay mineral (asphaltenes > resins > aromatics > aliphatics) may be the main reason (Sandvik et al., 1992; Han et al., 2015; Zou et al., 2019a). Adsorption of saturate hydrocarbon on TOC content and clays appears to be of less importance (Espitalie et al., 1980; Schettler and Parmely, 1991). The increase of organic matter content not only contributes to the generation and retention of hydrocarbons, but also promotes the adsorption of polar components (Fig. 12g). Generally, the residual oil components in the organic lean interval are mostly non–polar components, and the residual oil components in the organic rich interval and clay mineral rich interval are mostly aromatic hydrocarbons and polar components (Zou et al., 2019a). However, type C samples, the organic lean shale, have higher percentage of polar components (Fig. 12g, h and i). The polar components percentage of type C shale increases significantly with the increasing clay mineral content, and type C shale has a higher clay mineral content. Han et al. (2015) proposed that the higher clay mineral content can increase the adsorption capacity of polar components, which may be the reason for high polar components and low saturated hydrocarbon percentage in saline shale.

When the gypsum mineral content is less than 7.5%, the saturated hydrocarbon percentage in raw samples shows an upward trend (Fig. 12c), while the saturated hydrocarbon percentage increases slightly and tends to be gradually stable when the gypsum content exceeds 7.5% (Fig. 12c) with the increased fracture storage space (Fig. 10a, b and c). Therefore, shale with high gypsum mineral contents has more storage space for residual oil, especially contributing to the enrichment of the residual oil with high saturated hydrocarbons percentage in raw samples. It is worth noting that the gypsum content of sample d reaches 12.2% and the saturated hydrocarbon percentage in raw samples reaches 73.60%, but the $S_1$ value is only 0.67 mg/g (Fig. 12c). As mentioned above, the shale with high gypsum minerals content may be enriched in fractures (Wang et al., 2017), which may reduce the content of residual oil. However, the fractures of shale caused by the high gypsum content make the residual oil migrate between layers in shale system, and the saturated hydrocarbon percentage in raw samples increases relatively (Zou et al., 2019a). Therefore, the residual oil of sample d migrated from nearby shale reservoirs, and the preferential migration of saturated hydrocarbon caused the high percentage of saturated hydrocarbon.

Due to the high content of quartz in felsic minerals, so the effect of quartz minerals on the chemical composition of residual oil is mainly discussed. The saturated hydrocarbon percentage in raw samples increases with the increasing of quartz mineral content of

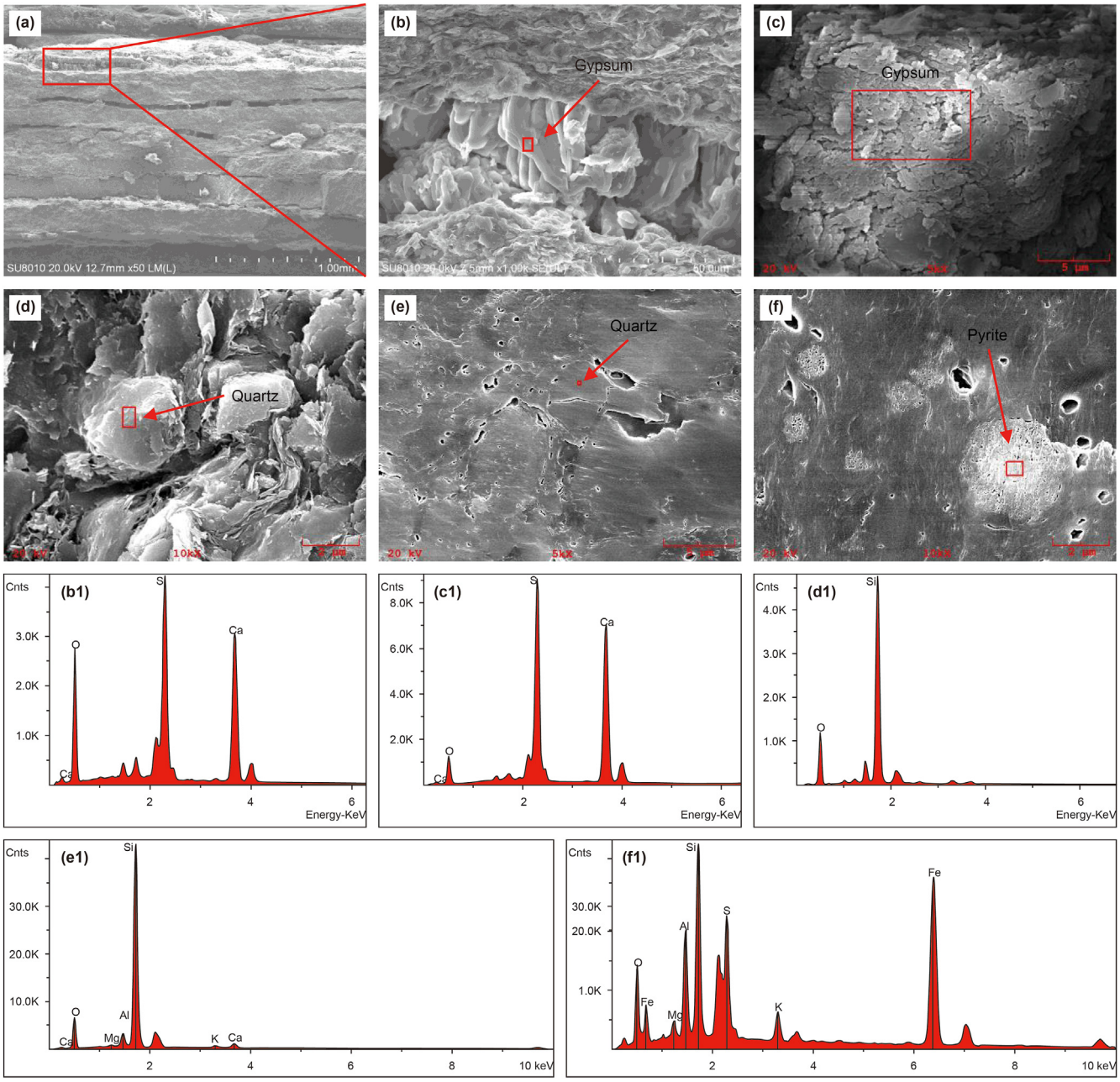


**Fig. 10.** Typical mineral of gypsum and quartz. (**a**) and (**b**): 2991.28 m, well W155, the gypsum minerals are developed in the middle of shale laminae; (**c**): 2991.28 m, well W155, the abundant gypsum minerals occur in the shale surface; (**d**) and (**e**): 3351.79 m, W248, nm–scale quartz cementation; (**f**): 2991.28 m, well W155, Intergranular pores of pyrite are filled with microcrystalline quartz. ($\mathbf{b_1}$): EDS analyses of the point marked red rectangle sign in Image (**b**); ($\mathbf{c_1}$): EDS analyses of the point marked red rectangle sign in Image (**c**); ($\mathbf{d_1}$): EDS analyses of the point marked red rectangle sign in Image (**d**); ($\mathbf{e_1}$): EDS analyses of the point marked red rectangle sign in Image (**e**); ($\mathbf{f_1}$): EDS analyses of the point marked red rectangle sign in Image (**f**).

which the maximum is 21.1% (Fig. 12j). The polar components percentage in type A and B shale decreases with the increase of quartz mineral content (Fig. 12l). When the quartz content is less than 21.1%, the residual oil content increases with the increasing of quartz content, resulting in the corresponding increase of saturated hydrocarbon percentage in raw samples (Fig. 9c and d). The quartz minerals have more interparticle pores at micron scale than clay minerals, resulting in the enrichment of aliphatic and aromatic compounds (Gorbanenko and Ligouis, 2014; Liu et al., 2020). The biogenic quartz-rich Barnett marine shale have high proportions of polar components (especially the resins fraction) retained in the Barnett samples due to the high adsorption capacity of the small inter-particle pores on biogenic quartz (Yue et al., 2021). But in this study, the intergranular pore formed by detrital quartz minerals is about 10–50 nm (Fig. 10d, e and f), leading to the reducing adsorption capacity of quartz minerals for polar components (Xi et al., 2019), and resulting in its favor of the fractionation and migration of residual oil (Shao et al., 2018). Therefore, the effect of gypsum and quartz on petroleum component fractionation of residual oil cannot be ignored.

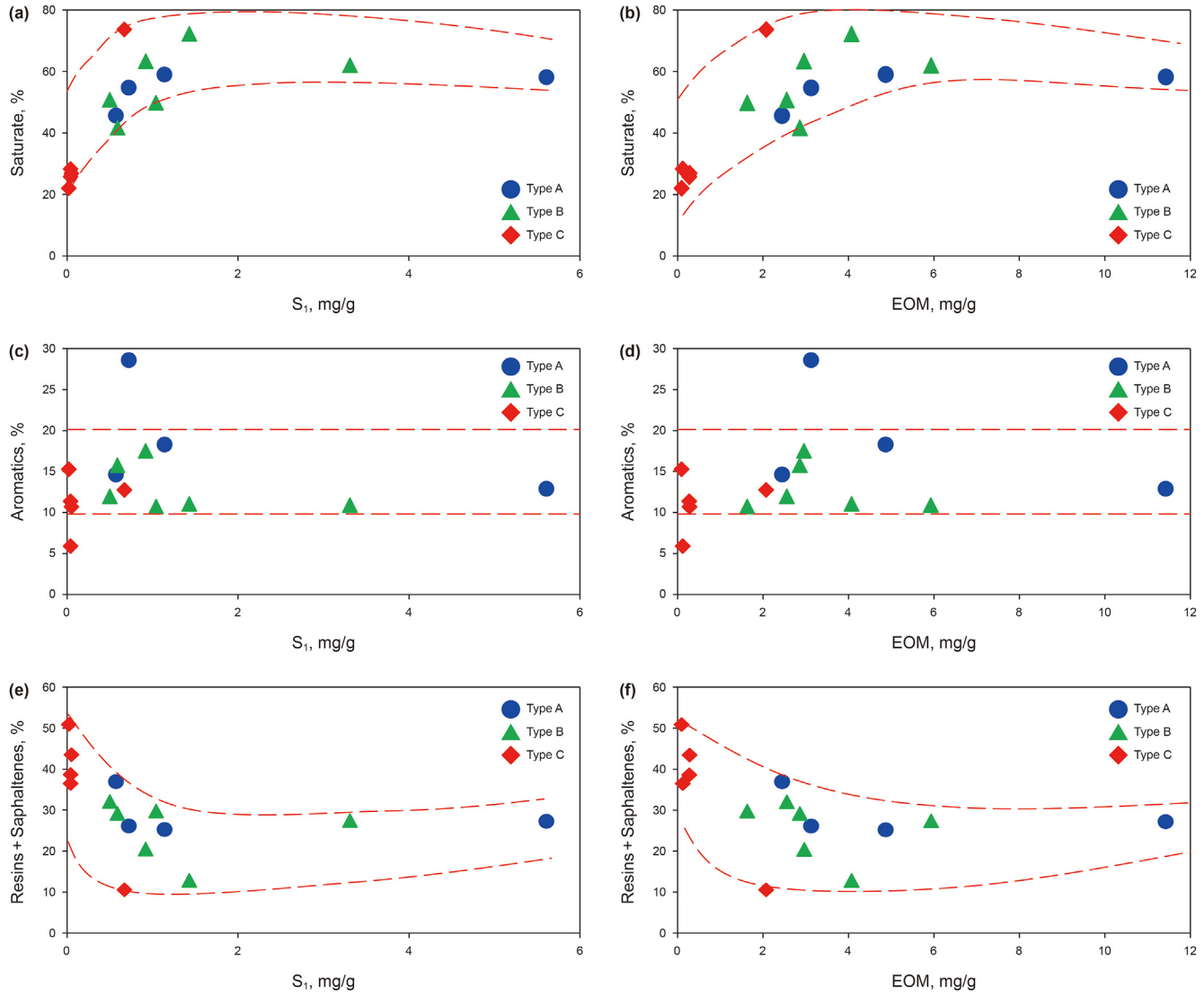


**Fig. 11.** The effect of $S_1$ and EOM on saturate, aromatic, resins and saphaltenes content of shale in the Dongpu Depression. (**a**) The effect of $S_1$ yield on saturate; (**b**) the effect of EOM yield on saturate; (**c**) the effect of $S_1$ yield on aromatics; (**d**) the effect of EOM yield on aromatics; (**e**) the effect of $S_1$ yield on the sum of resins and saphaltenes; (**f**) the effect of EOM yield on the sum of resins and saphaltenes.

### 5.3. Effect of maturity on residual oil

In the above discussion, the shale samples are basically in the mature stage. However, different thermal maturities may also affect the retention and component changes of residual oil (Snarsky, 1962; Pelet and Tissot, 1971; Zou et al., 2004). The thermal simulation experiment of closed system is adopted to analyze the changes of residual oil content and chemical composition under different thermal maturities.

#### 5.3.1. Residual oil and pore structure characteristic

The oil expulsion yield and gas generation yield vary intricately (Fig. 13a and b), which was divided into two stages: Stage I (320–360 °C) and Stage II (360–400 °C) (Table 2). In the Stage I and II, there is a downward trend of the residual oil yield, which may be attributed to the partial conversion of extractable asphalt into insoluble coking asphalt (Ertas et al., 2006; Wei et al., 2014). In addition, continuous oil expulsion can also lead to a continuous decrease in the residual oil content (Guo et al., 2017).

The $N_2$ adsorption and desorption are carried out for the shale before extraction (SBE) and the shale after extraction (SAE) (Table 3). IUPAC divides the adsorption isotherms into 6 types (I–VI), and the desorption isotherms (i.e. hysteresis curves) into 4 types (H1–H4) (Ross and Bustin, 2009). The nitrogen adsorption capacity of SBE and SAE increases with the increase of relative pressure (Fig. 14). The adsorption–desorption curve hysteresis loops of samples can be divided into type II and H3, respectively, indicating that the pores in shale are narrow shaping parallel plate pores, which are open in all directions (Sing, 1985). The adsorption capacity of samples increases significantly at $P/P_0 < 0.5$, indicating the process of single-layer adsorption of gas (Tang et al., 2017). When $P/P_0$ is greater than 0.5, the adsorption–desorption curve shows a lag loop (Mastalerz et al., 2013; Gou et al., 2019). When $P/P_0$ approaches 1, the adsorption capacity increases significantly and the horizontal platform disappears, indicating that there is a large number of macropores (Ravikovitch and Neimark, 2002).

The adsorption capacity of SAE is greater than that of SBE, indicating that the pore volume of SAE is larger (Fig. 15). In Stage I, the total pore volume of SAE increases by 1.4 times, the specific surface area increases by 2.2 times, and the average pore diameter

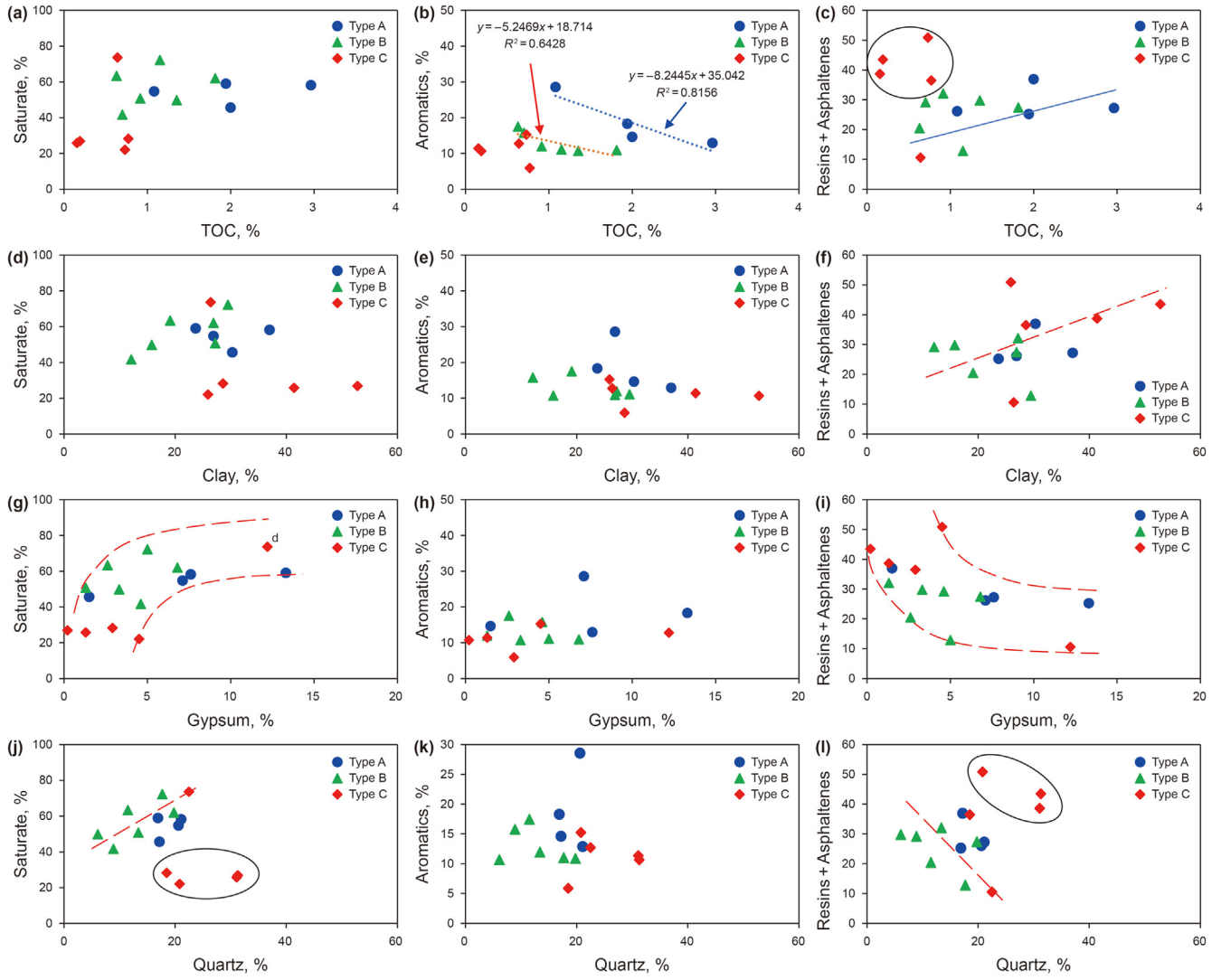


**Fig. 12.** The effect of TOC, clay and gypsum on saturate, aromatic, resins and saphaltenes content of shale in the Dongpu Depression. (**a**) The effect of TOC content on saturate; (**b**) the effect of clay mineral content on saturate; (**c**) the effect of gypsum mineral content on saturate; (**d**) the effect of TOC content on aromatics; (**e**) the effect of clay mineral content on aromatics; (**f**) the effect of gypsum mineral content on aromatics; (**g**) the effect of TOC content on the sum of resins and saphaltenes; (**h**) the effect of clay mineral content on the sum of resins and saphaltenes; (**i**) the effect of gypsum mineral content on the sum of resins and saphaltenes.

decreases by 20%–40%. In Stage II, the total pore volume of SAE maximum increases by 1.8 times, the specific surface area increases by 1.9 times, and the average pore diameter decreases by 20%–30% (Fig. 16). These indicate that the SAE in Stage II are more enriched in small pores. The difference of pore characteristics in SAE and SBE can characterize the occurrence characteristics of residual oil (Guo and Li, 2000; Li et al., 2020b).

In Stage I, the pores of SAE with pore width > 20 nm increase greatly, indicating that the residual oil mainly exists in these pores, including quartz mineral intergranular pores, calcite mineral intergranular pores and clay mineral pores (Fig. 17a, b, c and h). The difference in Stage II, the total pore volume and specific surface area of SAE and SBE, is greater than that in Stage I. These indicate that more mesopores (< 5 nm) which do not exist in Stage I appear in Stage II with the increasing temperature. The sudden increase of gas generation in Stage II may result from the existence of organic matter pores and mineral matrix corrosion pores that lead to a big increase of total pore volume and specific surface area in SAE (Löhr et al., 2015; Cao et al., 2020) (Fig. 17d, e, f and i). Most of the organic matter pores are formed by pyrite intergranular filling with organic matter. The organic matter biofilm around pyrite indicates a better chemical environment for the formation and preservation of pyrite (Zhu and Reinfelder, 2012). Pyrite can also promote the hydrocarbon generation, and facilitate the formation of organic pores (Ma et al., 2016; Cao et al., 2018). Studies on the Muskwa and Besa River shales in Northern British Columbia, western Canada, also implied that the organic matter content can contribute to the development of mesopores (Ross and Bustin, 2009; Dong et al., 2019). The average pore size of SAE and SBE has little difference, while the average pore size of shale in Stage II is lower than that in Stage I. Therefore, the increase of polar component percentage in Stage II may also result from the emergence of organic matter pores, which is conducive to the adsorption of polar components (Fig. 17d and e).

However, there is an exception in Stage I, that is, when the temperature is 360 °C, the total pore volume of SAE increases by only 1.09 times, the average pore diameter is the highest at 21.83 nm, and the specific surface area is the smallest at 2.36 $m^2/g$. These show that there are no organic matter pores, resulting in the decrease of specific surface area and increase of average pore size of

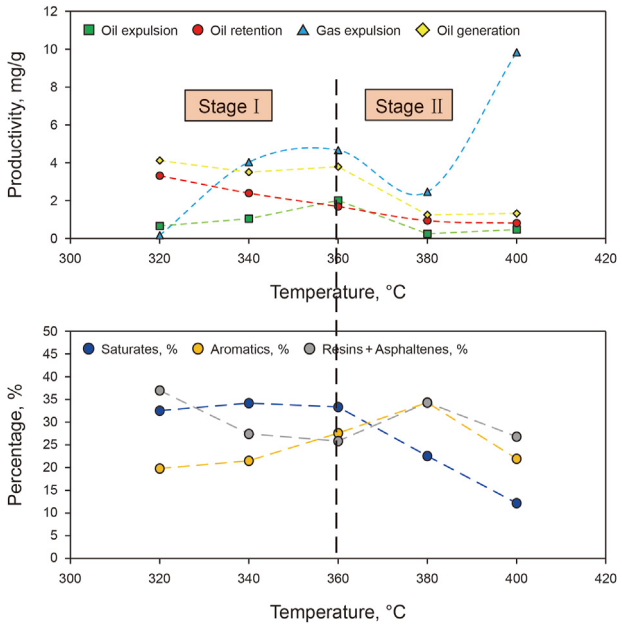


**Fig. 13.** (**a**) The oil generation, expulsion and retention yield, gas generation yield in different pyrolysis temperatures of shale; (**b**) The chemical component of residual oil in different pyrolysis temperature of shale.

SAE. Combined with the discussion in 5.2, polar components are preferentially adsorbed in the mineral pores and organic matter pores in the reservoir during the process of oil expulsion (Sandvik et al., 1992). In Stage I, many pores with pore width < 5 nm of SAE can be observed at 320–340 °C, while many pores with pore width less than 5 nm of SBE can be even found at 360 °C, and the minimum pore diameter of SAE is 8 nm at this moment (Fig. 16), which can be attributed to that the polar components of the residual oil are adsorbed on the pore surface, resulting in the smaller pore size of SBE and the larger pore size of SAE without the influence of residual oil. In Stage II, the pore volume of samples with pore diameter < 5 nm or > 20 nm increased after extraction, indicating that the residual oil exists in both types of pores at this stage.

### 5.3.2. The chemical component of residual oil

Stage I: The saturated hydrocarbon percentage of residual oil remains stable at 33%, while the oil expulsion yield increases from 0.67 mg/g to 2.01 mg/g, and the oil generation yield basically remains stable (3.50–4.12 mg/g) (Fig. 13). During the continuous transformation of kerogen into hydrocarbons, the saturated hydrocarbons percentage remains stable, and the aromatic hydrocarbons percentage increases from 19.82% to 27.59% (Fig. 13), but the polar components percentage decreases from 36.98% to 25.86% (Fig. 13). Previous studies have shown that asphalt is used as an intermediate product in the process of oil generation of type II

**Table 3**
The pore structure parameters of thermal simulation samples before and after extraction.

| | Samples before extration | | | Samples after extration | | |
|---|---|---|---|---|---|---|
| Temprature, °C | BET surface area, $m^2/g$ | Total pore volume, $cm^3/100g$ | Average pore width, nm | BET surface area, $m^2/g$ | Total pore volume, $cm^3/100g$ | Average pore width, nm |
| 320 | 2.79 | 1.53 | 19.77 | 5.23 | 2.00 | 17.69 |
| 340 | 2.08 | 1.27 | 29.36 | 4.67 | 1.81 | 18.63 |
| 360 | 2.70 | 1.03 | 17.45 | 2.36 | 1.12 | 21.83 |
| 380 | 3.60 | 1.37 | 18.11 | 7.05 | 2.00 | 13.10 |
| 400 | 3.91 | 1.41 | 16.87 | 7.74 | 2.52 | 14.49 |

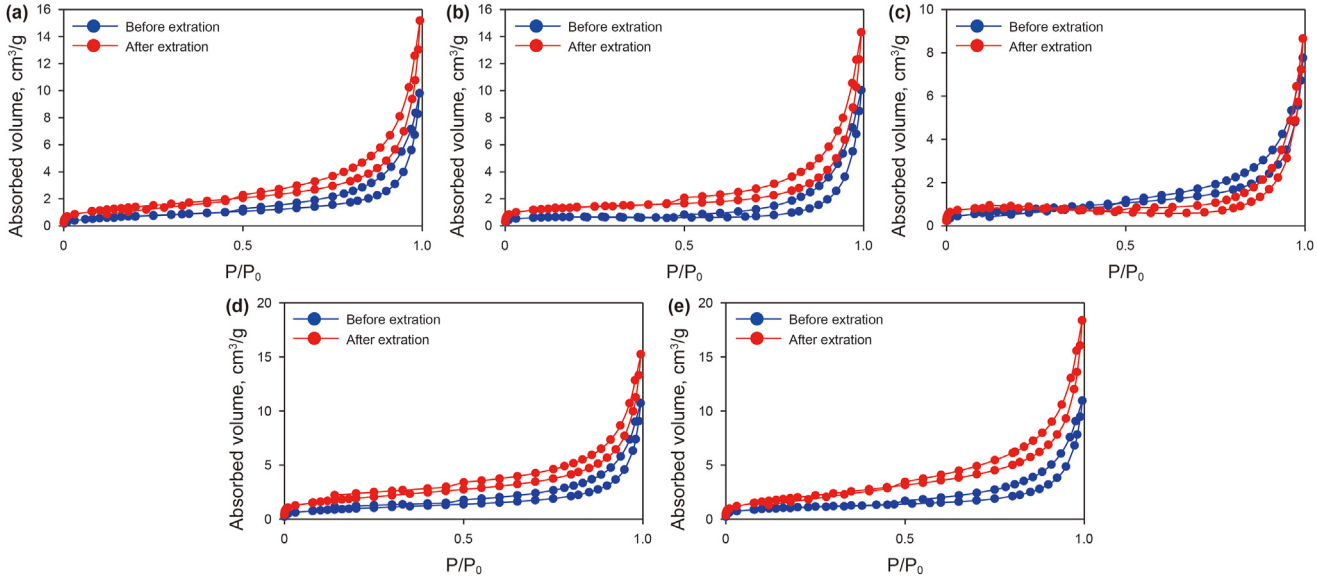


**Fig. 14.** The $N_2$ adsorption isotherm of the thermal simulation sample before and after extraction (the blue line and the red line); Simulated temperature: (**a**) 320 °C; (**b**) 340 °C; (**c**) 360 °C; (**d**) 380 °C; (**e**) 400 °C.

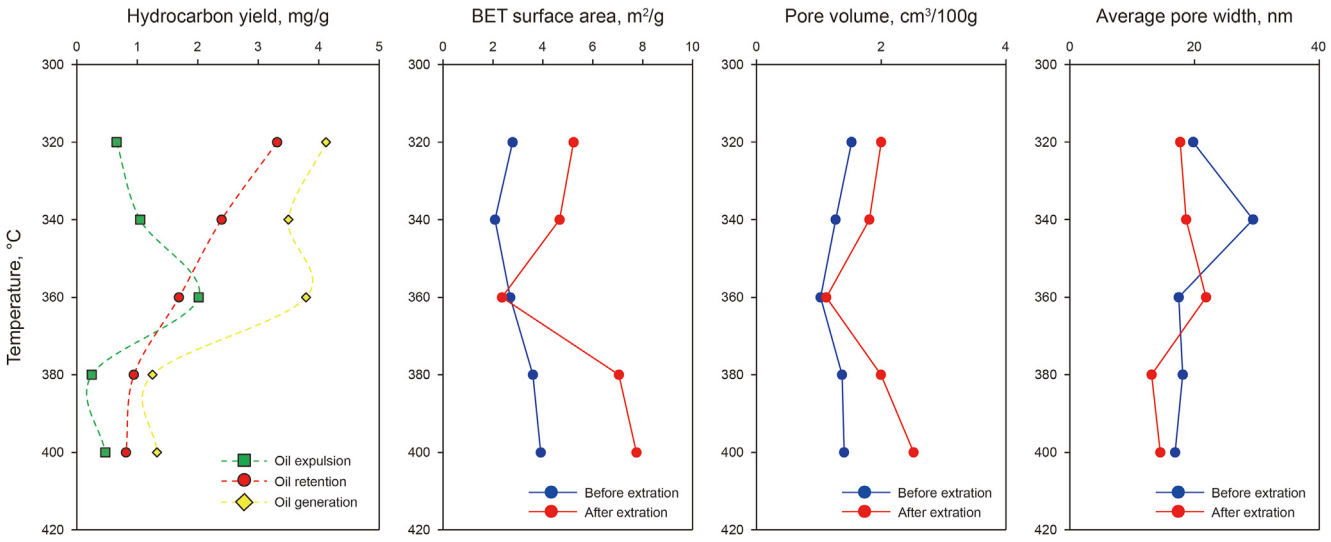


**Fig. 15.** The BET surface area, pore volume and average pore width of the sample before and after extraction in different pyrolysis temperatures.

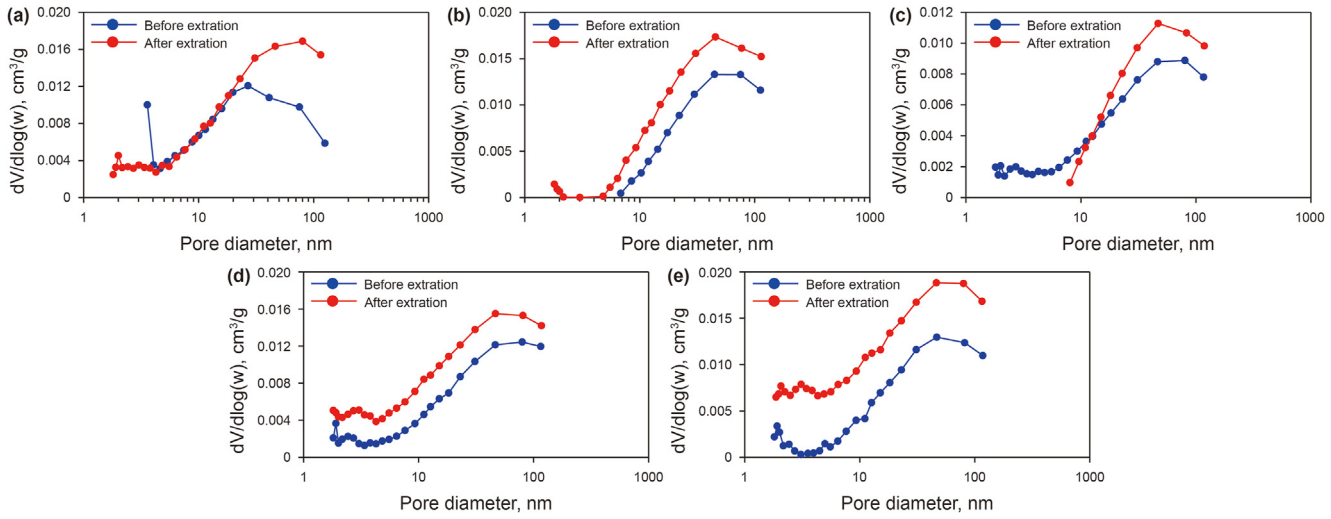


**Fig. 16.** The distribution of pore diameter of the sample before and after extraction; Simulated temperature: (**a**) 320 °C; (**b**) 340 °C; (**c**) 360 °C; (**d**) 380 °C; (**e**) 400 °C.

lacustrine kerogen (Lewan, 1997), and the asphalt composition here is roughly equivalent to the polar components in the present study (Song et al., 2020). During the continuous decomposition of kerogen, the consumption of asphalt occurs simultaneously with the large expulsion of oil (Behar et al., 2008; Lewan and Roy, 2012), and the polar components in the residual oil may become the main source of saturated hydrocarbons in the expulsion oil (Behar et al., 2010). Therefore, the oil expulsion has a great impact on the components in the shale residual oil at this moment (Wu et al., 2019).

Stage II:The residual oil decreased continuously, and the components are more complex (Fig. 13). The saturated hydrocarbon percentage significantly decreases from 33.33% to 12.2% (Fig. 13). At 360–380 °C, the oil generation and oil expulsion yields begin to decrease significantly, and the asphalts stored in shale pores begin to discharge hydrocarbons under the influence of the increasing temperature and pressure (Lafargue et al., 1990). Therefore, the saturated hydrocarbons percentage is preferentially discharged during the fractionation of chemical components of the residual oil (Leythaeuser et al., 1988; Pepper and Corvi, 1995; Ritter, 2003). However, aromatic hydrocarbons and polar compounds percentage follows a similar pattern, initially increasing and then decreasing. The transformation processes, kerogen → asphalt → oil, make the inner surface of source rock lipophilic (Lewan, 1993), accompanied with the microfracture (Fig. 17g) which increases the porosity and pore network interconnection of rock matrix (Jarvie et al., 2007; Ko et al., 2016). This lipophilicity of the kerogen surface can promote the further discharge of saturated hydrocarbons percentage, and also provide favorable storage conditions for aromatics and polar components (Ritter, 2003). At 380–400 °C, the saturated hydrocarbon percentage still decreases, and the resins and asphaltene percentage also start to decrease (Fig. 13), which may be related to the cracking of crude oil (Tissot and Welte, 1984). Most carboxylic acids (polar components) can crack into a large amount of gas at high temperature, and the rock can also expel hydrocarbons to the greatest extent (Shao et al., 2018b).

In this study, the retention mechanism and the fractionation characteristics of residual oil in saline shale have been revealed. The saline shale has high residual oil content and high saturated hydrocarbon percentage, which is conducive to the exploration and development of shale oil. In addition, the existence of gypsum

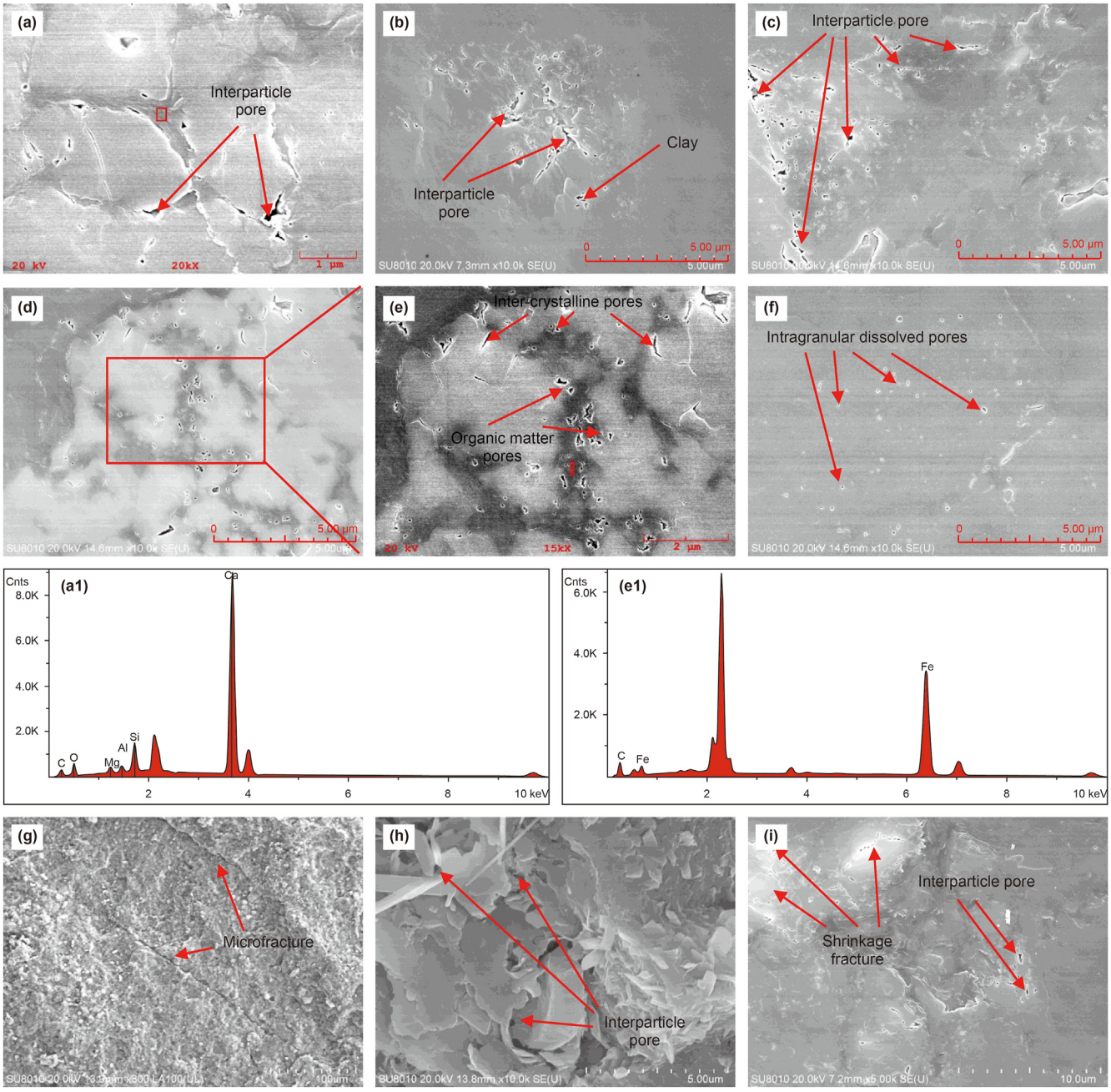


**Fig. 17.** Scanning electron microscopy (FE–SEM) of thermal simulation samples; (**a**) The pyrolysis temperature: 320 °C. The Interparticle pores of calcite; (**b**) The pyrolysis temperature: 360 °C. The Interparticle pores of clay; (**c**) The pyrolysis temperature: 340 °C. Interparticle pores; (**d**) and (**e**) The pyrolysis temperature: 380 °C. Inter-crystalline pores filled with organic matter and the organic matter pores; (**f**) The pyrolysis temperature: 400 °C. Intragranular dissolved pores; ($\mathbf{a_1}$): EDS analyses of the point marked red rectangle sign in Image (**a**); ($\mathbf{e_1}$): EDS analyses of the point marked red rectangle sign in Image (**e**); (**g**) The pyrolysis temperature: 400 °C. Microfractures; (**h**) The pyrolysis temperature: 360 °C. The Interparticle pores of clay; (**i**) The pyrolysis temperature: 360 °C. The shrinkage fracture and interparticle pores.

minerals is conducive to the formation of fractures in saline shale, which can guide the future exploration direction of shale oil in Dongpu Depression and other saline basins in China. The saline shale in this study only contains gypsum minerals, but there are many shale containing other salt minerals (including salt rock, alkaline mineral, etc.) in other saline basins in China, so the shale oil retention mechanism still needs to be deeply explored.

## 6. Conclusions

Typical saline lacustrine shales of the Member 3 of the Paleogene Shahejie Formation (43.59 ± 0.57 Ma to 36.08 ± 0.57 Ma) in the Dongpu Depression were taken to explore the main controlling factors on the residual oil content and its chemical fractionation in saline lacustrine shale. The TOC content is the key factor to control the residual oil content of saline shale, while clay minerals contents have little effect on the residual oil content of saline shale, which can be attributed to the high adsorption capacity reducing the reservoir porosity and permeability. However, the saline shale with high TOC content and clay mineral content is conducive to the adsorption of polar components. The intergranular pores of quartz (about 21.5%) and gypsum (about 7.5%) are

conducive to the occurrence of residual oil in saline shale, the increasing of saturated hydrocarbon percentage and the decreasing of polar components in the residual oil, which owe to the increasing migration channel caused by the preferential wettability of gypsum and interlayer fractures owing to too high content of brittle minerals.

The saline mature shale is in the main oil generation stage, which have higher residual oil content and shale oil potential. The residual oil mainly occurs in mesopores with pore diameter > 20 nm. The existence of gypsum minerals improves the pore connectivity, resulting in the high saturated hydrocarbon percentage and the gradual reduction of polar components of residual oil. In the gas generation stage, residual oil exists in mesopores which > 20 nm or < 5 nm. With the gradual cracking of the residual oil, the saturated hydrocarbon percentage decreases rapidly, and the polar component percentage begins to increase. There are also many organic matter pores which also provide storage space for residual oil.

## Credit authors statement

Chen-Xi Zhu: Conceptualization, Methodology, Software, Writing-Original draft preparation. Fu-Jie Jiang: Supervision. Peng-Yuan Zhang: Review & Editing. Zhao Zhao: Validation. Xin Chen: Validation. Yu-Qi Wu: Data curation. Yuan-Yuan Chen: Investigation. Wei Wang: Investigation. Tian-Wu Xu: Visualization. Yong-Shui Zhou: Visualization.

## Declaration of competing interest

The authors declare that they have no known competing financial interests or personal relationships that could have appeared to influence the work reported in this paper.

## Acknowledgements

This research was grateful to Sinopec Zhongyuan Oilfield Branch for providing experimental samples and allowing publication. This research was funded by the National Natural Science Foundation of China (NSFC) (41872128), the Science Foundation of China University of Petroleum, Beijing (No. 2462020YXZZ021).

## References

Anderson, G.M., 1977. Playas and dried lakes. Earth Sci. Rev. 13 (1), 66–67. https://doi.org/10.1016/0012-8252(77)90060-5.

Bao, Y.S., Zhang, L.Y., Zhang, J.G., et al., 2016. Factors influencing mobility of paleogene shale oil in Dongying sag, Bohai Bay Basin. Oil Gas J. 37, 408–414. https://doi.org/10.11743/ogg20160314 (in Chinese).

Barrett, E.P., Joyner, L.G., Halenda, P.P., 1951. The determination of pore volume and area distributions in porous substances. I. Computations from nitrogen isotherms. J. Am. Chem. Soc. 73 (1), 373–380. https://doi.org/10.1021/ja01145a126.

Behar, F., Lorant, F., Lewan, M., 2008. Role of NSO compounds during primary cracking of a Type II kerogen and a Type III lignite. Org. Geochem. 39 (1), 1–22. https://doi.org/10.1016/j.orggeochem.2007.10.007.

Behar, F., Roy, S., Jarvie, D., 2010. Artificial maturation of a Type I kerogen in closed system: mass balance and kinetic modelling. Org. Geochem. 41 (11), 1235–1247. https://doi.org/10.1016/j.orggeochem.2010.08.005.

Bjørlykke, K., 1997. Predictions of burial diagenetic reactions in sandstones and shales; importance for fluid flow and basin modeling. Am. Assoc. Petrol. Geol. 11–12.

Bjørlykke, K., 1998. Clay mineral diagenesis in sedimentary basins—a key to the prediction of rock properties. Examples from the North Sea Basin. Clay Miner. 33 (1), 15–34. https://doi.org/10.1180/000985598545390.

Bordenave, M.L., 1993. Geochemical methods and tools in petroleum exploration. In: Applied Petroleum Geochemistry. Editions Technip, Paris, pp. 207–216.

Brenneman, M.C., Smith Jr., P.V., 1958. The Chemical Relationships Between Crude Oils and Their Source Rocks: Topical Papers. AAPG Special Volumes, pp. 818–849.

Cao, T.T., Deng, M., Song, Z.G., et al., 2018. Study on the effect of pyrite on the accumulation of shale oil and gas. Nat. Gas Geosci. 29 (3), 404–414. https://doi.org/10.11764/j.issn.1672-1926.2017.12.006.

Cao, Y., Han, H., Guo, C., et al., 2020. Influence of extractable organic matters on pore structure and its evolution of Chang 7 member shales in the Ordos Basin, China: implications from extractions using various solvents. J. Nat. Gas Sci. Eng. 103370, 79. https://doi.org/10.1016/j.jngse.2020.103370.

Cardott, B.J., 2012. Thermal maturity of Woodford Shale gas and oil plays, Oklahoma, USA. Int. J. Coal Geol. 103, 109–119. https://doi.org/10.1016/j.coal.2012.06.004.

Cen, K., Zheng, X., Jiang, X., et al., 2016. A three-level optimization methodology for the partitioning of shale gas wellpad groups. J. Nat. Gas Sci. Eng. 34, 341–355. https://doi.org/10.1016/j.jngse.2016.07.009.

Chang, X., Xue, Q.Z., Li, X.F., et al., 2018. Inherent wettability of different rock surfaces at nanoscale: a theoretical study. Appl. Surf. Sci. 434, 73–81. https://doi.org/10.1016/j.apsusc.2017.10.173.

Chen, J.P., Zhao, C.Y., He, Z.H., 1997. Discussion on evaluation criteria for hydrocarbon generation potential of organic matter in coal measures. Petrol. Explor. Dev. 24 (1), 1–5 (in Chinese).

Chen, F.L., Zhu, H., Li, X.T., 2000. Partition of sequence strata and discussion about salt-rock resource in Shahejie Formation of Eogene, Dongpu depression. Acta Sedimentol. Sin. 18 (3), 384–388. https://doi.org/10.3969/j.issn.1000-0550.2000.03.010.

Chen, S.P., Xu, S.S., Wang, D.R., et al., 2013. Effect of block rotation on fault sealing: an example in Dongpu sag, Bohai Bay basin, China. Mar. Petrol. Geol. 39 (1), 39–47. https://doi.org/10.1016/j.marpetgeo.2012.10.002.

Chen, Y.Y., Lin, S.H., Bai, B., et al., 2020. Effects of petroleum retention and migration within the Triassic Chang 7 member of the Ordos basin, China. Int. J. Coal Geol. 103502, 225. https://doi.org/10.1016/j.coal.2020.103502.

Cooles, G.P., Mackenzie, A.S., Quigley, T.M., 1986. Calculation of petroleum masses generated and expelled from source rocks. Org. Geochem. 10 (1–3), 235–245. https://doi.org/10.1016/0146-6380(86)90026-4.

Dong, T., Harris, N.B., McMillan, J.M., et al., 2019. A model for porosity evolution in shale reservoirs: an example from the upper Devonian Duvernay formation, western Canada sedimentary basin. AAPG (Am. Assoc. Pet. Geol.) Bull. 103 (5), 1017–1044. https://doi.org/10.1306/1026181727.

Emmings, J.F., Hennissen, J.A.I., Stephenson, M.H., et al., 2019. Controls on amorphous organic matter type and sulphurization in a Mississippian black shale. Rev. Palaeobot. Palynol. 268, 1–18. https://doi.org/10.1016/j.revpalbo.2019.04.004.

Emmings, J.F., Poulton, S.W., Vane, C.H., et al., 2020. A Mississippian black shale record of redox oscillation in the Craven Basin, UK. Palaeogeogr. Palaeoclimatol. Palaeoecol. 109423, 538. https://doi.org/10.1016/j.palaeo.2019.109423.

Ertas, D., Kelemen, S.R., Halsey, T.C., 2006. Petroleum expulsion part 1. Theory of kerogen swelling in multicomponent solvents. Energy and Fuels 20 (1), 295–300. https://doi.org/10.1021/ef058024k.

Eseme, E., Littke, R., Krooss, B.M., et al., 2007. Experimental investigation of the compositional variation of petroleum during primary migration. Org. Geochem. 38 (8), 1373–1397. https://doi.org/10.1016/j.orggeochem.2007.03.003.

Espitalié, J., Madec, M., Tissot, B., et al., 1977. Source rock characterization method for petroleum exploration, Offshore Technology Conference. OnePetro 23–45.

Espitalie, J., Madec, M., Tissot, B., 1980. Role of mineral matrix in kerogen pyrolysis: influence on petroleum generation and migration. AAPG (Am. Assoc. Pet. Geol.) Bull. 64 (1), 59–66. https://doi.org/10.1306/2F918928-16CE-11D7-8645000102C1865D.

Fishman, N.S., Egenhoff, S.O., Boehlke, A.R., et al., 2015. Petrology and diagenetic history of the upper shale member of the late Devonian–early Mississippian Bakken formation, Williston basin, north Dakota. GSA (Geol. Soc. Am.) Spec. Pap. (Reg. Stud.) 515, 125–151. https://doi.org/10.1130/2015.2515(07).

Gao, H.C., Zheng, R.C., Chen, F.L., et al., 2011. Sequence stratigraphy of the paleogene Shahejie Formation in Dongpu Sag, Bohai Bay Basin. Oil Gas Geol. 32 (6), 839–850 (in Chinese).

Gorbanenko, O.O., Ligouis, B., 2014. Changes in optical properties of liptinite macerals from early mature to post mature stage in Posidonia Shale (Lower Toarcian, NW Germany). Int. J. Coal Geol. 133, 47–59. https://doi.org/10.1016/j.coal.2014.09.007.

Gorynski, K.E., Tobey, M.H., Enriquez, D.A., et al., 2019. Quantification and characterization of hydrocarbon-filled porosity in oil-rich shales using integrated thermal extraction, pyrolysis, and solvent extraction. AAPG (Am. Assoc. Pet. Geol.) Bull. 103 (3), 723–744. https://doi.org/10.1306/08161817214.

Gou, Q.Y., Xu, S., Hao, F., et al., 2019. Full-scale pores and micro-fractures characterization using FE-SEM, gas adsorption, nano-CT and micro-CT: a case study of the Silurian Longmaxi Formation shale in the Fuling area, Sichuan Basin, China. Fuel 253, 167–179. https://doi.org/10.1016/j.fuel.2019.04.116.

Grice, K., Schouten, S., Peters, K.E., et al., 1998. Molecular isotopic characterisation of hydrocarbon biomarkers in Palaeocene-Eocene evaporitic, lacustrine source rocks from the Jianghan Basin, China. Org. Geochem. 5, 1745–1764. https://doi.org/10.1016/S0146-6380(98)00075-8.

Grosjean, E., Love, G.D., Stalvies, C., et al., 2009. Origin of petroleum in the Neoproterozoic–Cambrian south Oman salt basin. Org. Geochem. 40 (1), 87–110. https://doi.org/10.1016/j.orggeochem.2008.09.011.

Guan, M., Liu, X.P., Jin, Z.J., et al., 2020. The heterogeneity of pore structure in lacustrine shales: insights from multifractal analysis using N2 adsorption and mercury intrusion. Mar. Petrol. Geol. 104150, 114. https://doi.org/10.1016/j.marpetgeo.2019.104150.

Guo, D., Jin, Z.J., 2021. Astronomical time scale of a middle Eocene lacustrine sequence from the Dongpu sag, Bohai Bay Basin, eastern China. J. Asian Earth

Sci. 104747, 214. https://doi.org/10.1016/j.jseaes.2021.104747.
Guo, S.H., Li, S.Y., Qin, K.Z., 2000. CS2/NMP extraction of immature source rock concentrates. Org. Geochem. 31 (12), 1783–1795. https://doi.org/10.1016/S0146-6380(00)00126-1.
Guo, H.J., Jia, W.L., Peng, P.A., et al., 2017. Evolution of organic matter and nanometer-scale pores in an artificially matured shale undergoing two distinct types of pyrolysis: a study of the Yanchang Shale with Type II kerogen. Org. Geochem. 105, 56–66. https://doi.org/10.1016/j.orggeochem.2017.01.004.
Hackley, P.C., SanFilipo, J.R., 2016. Organic petrology and geochemistry of Eocene Suzak bituminous marl, north-central Afghanistan: depositional environment and source rock potential. Mar. Petrol. Geol. 73, 572–589. https://doi.org/10.1016/j.marpetgeo.2016.02.029.
Hafiz, M., Hakhoo, N., Bhat, G.M., et al., 2020. Source potential and reservoir characterization of the Cambay Shale, Cambay Basin, India: implications for tight gas and tight oil resource development. AAPG (Am. Assoc. Pet. Geol.) Bull. 104 (8), 1707–1749. https://doi.org/10.1306/03162017174.
Han, Y.J., Mahlstedt, N., Horsfield, B., 2015. The Barnett Shale: compositional fractionation associated with intraformational petroleum migration, retention, and expulsion. AAPG (Am. Assoc. Pet. Geol.) Bull. 99 (12), 2173–2202. https://doi.org/10.1306/06231514113.
Han, Y.J., Horsfield, B., Wirth, R., et al., 2017. Oil retention and porosity evolution in organic-rich shales. AAPG Bulletin 101 (6), 807–827. https://doi.org/10.1306/09221616069.
Hao, F., Zou, H.Y., Gong, Z.S., et al., 2007. Petroleum migration and accumulation in the Bozhong sub-basin, Bohai Bay basin, China: significance of preferential petroleum migration pathways (PPMP) for the formation of large oilfields in lacustrine fault basins. Mar. Petrol. Geol. 24 (1), 1–13. https://doi.org/10.1016/j.marpetgeo.2006.10.007.
He, T.H., Lu, S.F., Li, W.H., et al., 2018. Effect of salinity on source rock formation and its control on the oil content in shales in the Hetaoyuan formation from the Biyang depression, Nanxiang basin, Central China. Energy and Fuels 32 (6), 6698–6707. https://doi.org/10.1021/acs.energyfuels.8b01075.
Hou, G.T., Qian, X.L., Cai, D.S., 2001. Study on Meso Cenozoic tectonic evolution in Bohai Bay Basin. J. Univ. Petrol. China 37, 845–851 (in Chinese).
Hou, Y.G., Wang, F.R., He, S., et al., 2017. Properties and shale oil potential of saline lacustrine shales in the Qianjiang Depression, Jianghan Basin, China. Mar. Petrol. Geol. 86, 1173–1190. https://doi.org/10.1016/j.marpetgeo.2017.07.008.
Hu, S.Z., Li, S.F., Xia, L.W., et al., 2020. On the internal oil migration in shale systems and implications for shale oil accumulation: a combined petrological and geochemical investigation in the Eocene Nanxiang Basin, China. J. Petrol. Sci. Eng. 106493, 184. https://doi.org/10.1016/j.petrol.2019.106493.
Hu, T., Pang, X.Q., Jiang, F.J., et al., 2021a. Movable oil content evaluation of lacustrine organic-rich shales: methods and a novel quantitative evaluation model. Earth Sci. Rev. 103545, 214. https://doi.org/10.1016/j.earscirev.2021.103545.
Hu, T., Pang, X.Q., Jiang, F.J., et al., 2021b. Key factors controlling shale oil enrichment in saline lacustrine rift basin: implications from two shale oil wells in Dongpu Depression, Bohai Bay Basin. Petrol. Sci. 18 (3), 687–711. https://doi.org/10.1007/s12182-021-00564-z.
Hu, T., Pang, X.Q., Jiang, F.J., et al., 2022a. Dynamic continuous hydrocarbon accumulation (DCHA): existing theories and a new unified accumulation model. Earth Sci. Rev. 104109, 232. https://doi.org/10.1016/j.earscirev.2022.104109.
Hu, T., Pang, X.Q., Xu, T.W., et al., 2022b. Identifying the key source rocks in heterogeneous saline lacustrine shales: paleogene shales in the Dongpu depression, Bohai Bay Basin, eastern China. AAPG (Am. Assoc. Pet. Geol.) Bull. 106 (6), 1325–1356. https://doi.org/10.1306/01202218109.
Huang, D.F., Li, J.C., Zhang, D.J., 1984. Kerogen types and study on effectiveness, limitation and interrelation of their identification parameters. Acta Sedimentol. Sin. 2 (3), 18–33 (in Chinese).
Huang, D.F., Zhang, D.J., Zhang, L.Y., 2003. Genetic Mechanism and Reservoir Forming Conditions of Immature Petroleum in China. Petroleum Industry Press, Beijing.
Huang, C.Y., Zhang, J.C., Hua, W., et al., 2018. Sedimentology and lithofacies of lacustrine shale: a case study from the Dongpu sag, Bohai Bay Basin, Eastern China. J. Nat. Gas Sci. Eng. 60, 174–189. https://doi.org/10.1016/j.jngse.2018.10.014.
Huang, Z.K., Liang, T., Zhan, Z.W., et al., 2018. Chemical structure evolution of kerogen during oil generation. Mar. Petrol. Geol. 98, 422–436. https://doi.org/10.1016/j.marpetgeo.2018.08.039.
Huang, C., Hou, H.J., Yu, G., et al., 2020. Energy solutions for producing shale oil: characteristics of energy demand and economic analysis of energy supply options. Energy 192, 116603. https://doi.org/10.1016/j.energy.2019.116603.
Jarvie, D.M., 2012. Shale resource systems for oil and gas: Part 2— Shale-oil resource systems. In: Breyer, J.A. (Ed.), Shale reservoirs—Giant resources for the 21st century, 97. AAPG Memoir, pp. 89–119. https://doi.org/10.1306/13321447M973489.
Jarvie, D.M., 2014. Components and processes affecting producibility and commerciality of shale resource systems. Geol. Acta: Int. Earth Sci. J. 12 (4), 307–325. https://doi.org/10.1344/GeologicaActa2014.12.4.3.
Jarvie, D.M., 2015. Geochemical assessment of unconventional shale gas resource systems. Fund. Gas Shale Reserv. 47–69. https://doi.org/10.1002/9781119039228.ch3.
Jarvie, D.M., Hill, R.J., Ruble, T.E., et al., 2007. Unconventional shale-gas systems: the Mississippian Barnett Shale of north-central Texas as one model for thermogenic shale-gas assessment. AAPG (Am. Assoc. Pet. Geol.) Bull. 91 (4), 475–499. https://doi.org/10.1306/12190606068.
Jia, C.Z., He, D.F., Lu, J.M., 2004. Episodes and geodynamic setting of Himalayan movement in China. Oil Gas Geol. 25, 121–125. https://doi.org/10.11743/ogg20040201.
Jia, C.Z., Zou, C.N., Li, J.Z., et al., 2016. Evaluation criteria, major types, characteristics and resource prospects of tight oil in China. Petrol. Res. 1 (1), 1–9. https://doi.org/10.1016/S2096-2495(17)30026-1.
Jiang, J.G., Peng, P.A., Sheng, G.Y., 2004. Formation, Evolution, Migration and Accumulation of Oil and Gas in Salt Lake. Guangdong science and Technology Press, Guangzhou.
Jiang, F.J., Pang, X.Q., Bai, J., et al., 2016a. Comprehensive assessment of source rocks in the Bohai Sea area, eastern China. AAPG (Am. Assoc. Pet. Geol.) Bull. 100 (6), 969–1002. https://doi.org/10.1306/02101613092.
Jiang, Z.X., Zhang, W.Z., Liang, C., et al., 2016b. Basic characteristics and evaluation of shale oil reservoirs. Petrol. Res. 1 (2), 149–163. https://doi.org/10.1016/S2096-2495(17)30039-X.
Jiang, F.J., Pang, X.Q., Li, L.L., et al., 2018. Petroleum resources in the Nanpu sag, Bohai Bay Basin, eastern China. AAPG (Am. Assoc. Pet. Geol.) Bull. 102 (7), 1213–1237. https://doi.org/10.1306/0906171608017148.
Jiang, F.J., Hu, T., Liu, L.F., et al., 2019. Geochemical and geological characteristics of the jurassic continental black shale in the southwestern depression of Tarim basin. Geol. J. 54 (3), 1115–1131. https://doi.org/10.1002/gj.3212.
Jiao, D.Q., Li, M., Mu, X.S., et al., 2014. Evolution of paleo-hydrodynamics and hydrocarbon migration and accumulation in southern Dongpu sag, Bohai Bay Basin. Oil Gas Geol. 35 (5), 585–594. https://doi.org/10.11743/ogg20140501 (in Chinese).
Jin, Q., Zhu, G.Y., Wang, J., 2008. Deposition and distribution of high-potential source rocks in saline lacustrine environments. J. China Univ. Petrol. (Ed. Nat. Sci.) 32 (4), 19–24. https://doi.org/10.3321/j.issn:1673-5005.2008.04.004 (in Chinese).
van de Kamp, P.C., 2008. Smectite-illite-muscovite transformations, quartz dissolution, and silica release in shales. Clays Clay Miner. 56 (1), 66–81. https://doi.org/10.1346/CCMN.2008.0560106.
Kelemen, S.R., Walters, C.C., Ertas, D., et al., 2006. Petroleum expulsion part 3. A model of chemically driven fractionation during expulsion of petroleum from kerogen. Energy and Fuels 20 (1), 309–319. https://doi.org/10.1021/ef058023s.
Ko, L.T., Loucks, R.G., Zhang, T.W., et al., 2016. Pore and pore network evolution of Upper Cretaceous Boquillas (Eagle Ford–equivalent) mudrocks: results from gold tube pyrolysis experiments. AAPG (Am. Assoc. Pet. Geol.) Bull. 100 (11), 1693–1722. https://doi.org/10.1306/04151615092.
Lafargue, E., Espitalie, J., Jacobsen, T., et al., 1990. Experimental simulation of hydrocarbon expulsion. Org. Geochem. 16 (1–3), 121–131. https://doi.org/10.1016/0146-6380(90)90032-U.
Larsen, J.W., Li, S., 1997. Changes in the macromolecular structure of a type I kerogen during maturation. Energy and Fuels 11 (4), 897–901. https://doi.org/10.1021/ef970007a.
Laughrey, C.D., Lemmens, H., Ruble, T.E., et al., 2009. Black shale diagenesis: insights from integrated high-definition analyses of post-mature Marcellus formation rocks. Northeastern Pennsylvania, PAPG Meeting 5–10.
Lewan, M.D., 1985. Evaluation of petroleum generation by hydrous phrolysis experimentation. Phil. Trans. Roy. Soc. London. Ser. A, Math. Phys. Sci. 315 (1531), 123–134. https://doi.org/10.1098/rsta.1985.0033.
Lewan, M.D., 1993. Laboratory Simulation of Petroleum formationOrganic Geochemistry. Springer, pp. 419–442.
Lewan, M.D., 1997. Experiments on the role of water in petroleum formation. Geochem. Cosmochim. Acta 61 (17), 3691–3723. https://doi.org/10.1016/S0016-7037(97)00176-2.
Lewan, M.D., Roy, S., 2012. Role of water in hydrocarbon generation from Type-I kerogen in Mahogany oil shale of the Green River Formation. Org. Geochem. 42 (1), 31–41. https://doi.org/10.1016/j.orggeochem.2010.10.004.
Lewan, M.D., Ruble, T.E., 2002. Comparison of petroleum generation kinetics by isothermal hydrous and nonisothermal open-system pyrolysis. Org. Geochem. 33 (12), 1457–1475. https://doi.org/10.1016/S0146-6380(02)00182-1.
Lewan, M.D., Dolan, M.P., Curtis, J.B., 2014. Effects of smectite on the oil-expulsion efficiency of the Kreyenhagen Shale, San Joaquin Basin, California, based on hydrous-pyrolysis experiments. AAPG Bull. 98 (6), 1091–1109. https://doi.org/10.1306/10091313059.
Leythaeuser, D., Schaefer, R.G., 1984. Effects of hydrocarbon expulsion from shale source rocks of high maturity in upper carboniferous strata of the Ruhr area, Federal Republic of Germany. Org. Geochem. 6, 671–681. https://doi.org/10.1016/0146-6380(84)90088-3.
Leythaeuser, D., Schaefer, R.G., Radke, M., 1987. SP2 on the primary migration of petroleum. 12th World Petrol. Congr. OnePetro 227–236.
Leythaeuser, D., Radke, M., Willsch, H., 1988. Geochemical effects of primary migration of petroleum in Kimmeridge source rocks from Brae field area, North Sea. II: molecular composition of alkylated naphthalenes, phenanthrenes, benzo-and dibenzothiophenes. Geochem. Cosmochim. Acta 52 (12), 2879–62891. https://doi.org/10.1016/0016-7037(88)90155-X.
Li, Z., Zou, Y.R., Xu, X.Y., et al., 2016. Adsorption of mudstone source rock for shale oil–Experiments, model and a case study. Org. Geochem. 92, 55–62. https://doi.org/10.1016/j.orggeochem.2015.12.009.
Li, L., Liu, Z.Z., George, S.C., et al., 2019. Lake evolution and its influence on the formation of oil shales in the middle jurassic shimengou Formation in the Tuanyushan area, Qaidam Basin, NW China. Geochemistry 79 (1), 162–177. https://doi.org/10.1016/j.geoch.2018.12.006.
Li, W.W., Cao, J., Shi, C.H., et al., 2020a. Shale oil in saline lacustrine systems: a perspective of complex lithologies of fine-grained rocks. Mar. Petrol. Geol. 104351, 116. https://doi.org/10.1016/j.marpetgeo.2020.104351.

Li, X., Cai, J.G., Liu, H.M., et al., 2020b. Characterization of shale pore structure by successive pretreatments and its significance. Fuel 117412, 269. https://doi.org/10.1016/j.fuel.2020.117412.

Li, W.D., Zhang, P.Y., Jiang, F.J., et al., 2021. Hydrocarbon generation characteristics of source rocks from different saline environments in the Dongpu depression, Bohai Bay Basin, China. Acta Geol. Sinica-English Ed. 95 (4), 1260–1278. https://doi.org/10.1111/1755-6724.14744.

Liang, C., Jiang, Z.X., Cao, Y.C., et al., 2017. Sedimentary characteristics and origin of lacustrine organic-rich shales in the salinized Eocene Dongying Depression. GSA Bulletin 130 (1–2), 154–174. https://doi.org/10.1130/B31584.1.

Lin, L.M., Zhang, J.C., Li, Y.X., et al., 2013. The potential of China's lacustrine shale gas resources. Energy Explor. Exploit. 31 (2), 317–335. https://doi.org/10.1260/0144-5987.31.2.317.

Lindgreen, H., Jacobsen, H., Jakobsen, H.J., 1991. Diagenetic structural transformations in North Sea Jurassic illite/smectite. Clay Clay Miner. 39 (1), 54–69. https://doi.org/10.1346/ccmn.1991.0390108.

Liu, C.L., Wang, Z.L., Guo, Z.Q., et al., 2017. Enrichment and distribution of shale oil in the cretaceous Qingshankou Formation, Songliao basin, northeast China. Mar. Petrol. Geol. 86, 751–770. https://doi.org/10.1016/j.marpetgeo.2017.06.034.

Liu, B., Yan, M., Sun, X.D., et al., 2020. Microscopic and fractal characterization of organic matter within lacustrine shale reservoirs in the first member of Cretaceous Qingshankou Formation, Songliao Basin, Northeast China. J. Earth Sci. 31 (6), 1241–1250. https://doi.org/10.1007/s12583-020-1345-3.

Löhr, S.C., Baruch, E.T., Hall, P.A., et al., 2015. Is organic pore development in gas shales influenced by the primary porosity and structure of thermally immature organic matter? Org. Geochem. 87, 119–132. https://doi.org/10.1016/j.orggeochem.2015.07.010.

López-Gamundí, O., 2010. Sedimentation styles and variability of organic matter types in the Triassic, non-marine half-grabens of west Argentina: implications for petroleum systems in rift basins. Petrol. Geosci. 16 (3), 267–272. https://doi.org/10.1144/1354-079309-912.

Luo, R., Cheng, T., Wang, P., et al., 2011. Research on types of organic matter of hydrocarbon source rocks in Kongdian Formation in Weibei depression. J. Chongqing Univ. Sci. Technol. (Nat. Sci. Ed.) 15, 69–71. https://doi.org/10.3969/j.issn.1673-1980.2011.06.020 (in Chinese).

Lyu, X.Y., Jiang, Y.L., 2017. Genesis of paleogene gas in the Dongpu depression, Bohai Bay Basin, east China. J. Petrol. Sci. Eng. 156, 181–193. https://doi.org/10.1016/j.petrol.2017.05.021.

Ma, X.X., Zheng, J.J., Zheng, G.D., et al., 2016. Influence of pyrite on hydrocarbon generation during pyrolysis of type-III kerogen. Fuel 167, 329–336. https://doi.org/10.1016/j.fuel.2015.11.069.

Manzi, V., Roveri, M., Gennari, R., et al., 2007. The deep-water counterpart of the Messinian lower evaporites in the apennine foredeep: the Fanantello section (Northern Apennines, Italy). Palaeogeogr. Palaeoclimatol. Palaeoecol. 251 (3–4), 470–499. https://doi.org/10.1016/j.palaeo.2007.04.012.

Mastalerz, M., Schimmelmann, A., Drobniak, A., et al., 2013. Porosity of Devonian and Mississippian New Albany Shale across a maturation gradient: insights from organic petrology, gas adsorption, and mercury intrusion. AAPG Bull. 97 (10), 1621–1643. https://doi.org/10.1306/04011312194.

Merriman, R.J., 1999. Patterns of very low-grade metamorphism in metapelitic rocks. Robinson Low-Grade Metamorphism Blackwell Sci. Oxford 61–107.

Milliken, K.L., Olson, T., 2017. Silica diagenesis, porosity evolution, and mechanical behavior in siliceous mudstones, Mowry Shale (Cretaceous), Rocky Mountains, USA. J. Sediment. Res. 87 (4), 366–387. https://doi.org/10.2110/jsr.2017.24.

Molnar, P., Tapponnier, P., 1975. Cenozoic Tectonics of Asia: effects of a Continental Collision: features of recent continental tectonics in Asia can be interpreted as results of the India-Eurasia collision. Science 189 (4201), 419–426. https://doi.org/10.1126/science.189.4201.419.

Mondol, N.H., Bjørlykke, K., Jahren, J., et al., 2007. Experimental mechanical compaction of clay mineral aggregates—changes in physical properties of mudstones during burial. Mar. Petrol. Geol. 24 (5), 289–311. https://doi.org/10.1016/j.marpetgeo.2007.03.006.

Ning, C.X., Ma, Z.L., Jiang, Z.X., et al., 2020. Effect of shale reservoir characteristics on shale oil movability in the lower third member of the Shahejie Formation, Zhanhua Sag. Acta Geol. Sinica-English Ed. 94 (2), 352–363. https://doi.org/10.1111/1755-6724.14284.

Nygård, R., Gutierrez, M., Gautam, R., et al., 2004. Compaction behavior of argillaceous sediments as function of diagenesis. Mar. Petrol. Geol. 21 (3), 349–362. https://doi.org/10.1016/j.marpetgeo.2004.01.002.

Oelkers, E.H., Bjorkum, P.A., Murphy, W.M., 1996. A petrographic and computational investigation of quartz cementation and porosity reduction in North Sea sandstones. Am. J. Sci. 296 (4), 420–452. https://doi.org/10.2475/ajs.296.4.420.

Pang, H., Pang, X.Q., Dong, L., et al., 2018. Factors impacting on oil retention in lacustrine shale: permian lucaogou Formation in Jimusaer depression, Junggar basin. J. Petrol. Sci. Eng. 163, 79–90. https://doi.org/10.1016/j.petrol.2017.12.080.

Pelet, R., Tissot, B., 1971. Nouvelles donnees sur les mecanismes de genese et de migration du petrole simulation mathematique et application a la prospection. 8th World Petrol. Congr. OnePetro 35–46.

Peltonen, C., Marcussen Ø, Bjørlykke K., et al., 2009. Clay mineral diagenesis and quartz cementation in mudstones: the effects of smectite to illite reaction on rock properties. Mar. Petrol. Geol. 26 (6), 887–898. https://doi.org/10.1016/j.marpetgeo.2008.01.021.

Pepper, A.S., 1991. Estimating the petroleum expulsion behaviour of source rocks: a novel quantitative approach Geological Society. London, Special Publications 59 (1), 9–31. https://doi.org/10.1144/GSL.SP.1991.059.01.02.

Pepper, A.S., Corvi, P.J., 1995. Simple kinetic models of petroleum formation. Part I: oil and gas generation from kerogen. Mar. Petrol. Geol. 12 (3), 291–319. https://doi.org/10.1016/0264-8172(95)98381-E.

Peters, K.E., 1986. Guidelines for evaluating petroleum source rock using programmed pyrolysis. AAPG Bull. 70 (3), 318–329. https://doi.org/10.1306/94885688-1704-11D7-8645000102C1865D.

Peters, K.E., Cunningham, A.E., Walters, C.C., et al., 1996. Petroleum systems in the Jiangling-Dangyang area, Jianghan basin, China. Org. Geochem. 24 (10–11), 1035–1060. https://doi.org/10.1016/S0146-6380(96)00080-0.

Qi, J.F., Yang, Q., 2010. Cenozoic structural deformation and dynamic processes of the Bohai Bay basin province, China. Mar. Petrol. Geol. 27 (4), 757–771. https://doi.org/10.1016/j.marpetgeo.2009.08.012.

Qu, X.R., Zhu, Y.M., Li, W., et al., 2018. Evaluation of hydrocarbons generated from the permo–carboniferous source rocks in Huanghua depression of the Bohai Bay Basin, China. Energy Explor. Exploit. 36 (5), 1229–1244. https://doi.org/10.1177/0144598718755465.

Radke, M., Willsch, H., Welte, D.H., 1980. Preparative hydrocarbon group type determination by automated medium pressure liquid chromatography. Anal. Chem. 52 (3), 406–411. https://doi.org/10.1021/ac50053a009.

Ravikovitch, P.I., Neimark, A.V., 2002. Experimental confirmation of different mechanisms of evaporation from ink-bottle type pores: equilibrium, pore blocking, and cavitation. Langmuir 18 (25), 9830–9837. https://doi.org/10.1021/la026140z.

Ritter, U., 2003. Solubility of petroleum compounds in kerogen: implications for petroleum expulsion. Org. Geochem. 34 (3), 319–326. https://doi.org/10.1016/S0146-6380(02)00245-0.

Rodriguez, N.D., Philp, R.P., 2010. Geochemical characterization of gases from the Mississippian Barnett shale, Fort worth basin. Texas. AAPG bulletin 94 (11), 1641–1656. https://doi.org/10.1306/04061009119.

Ross, D.J.K., Bustin, R.M., 2009. The importance of shale composition and pore structure upon gas storage potential of shale gas reservoirs. Mar. Petrol. Geol. 26 (6), 916–927. https://doi.org/10.1016/j.marpetgeo.2008.06.004.

Rouquerol, J., Llewellyn, P., Rouquerol, F., 2007. Is the BET equation applicable to microporous adsorbents. Stud. Surf. Sci. Catal. 160 (7), 49–56. https://doi.org/10.1016/s0167-2991(07)80008-5.

Salehi, M., Johnson, S.J., Liang, J.T., 2008. Mechanistic study of wettability alteration using surfactants with applications in naturally fractured reservoirs. Langmuir 24 (24), 14099–14107. https://doi.org/10.1021/la802464u.

Sandvik, E.I., Young, W.A., Curry, D.J., 1992. Expulsion from hydrocarbon sources: the role of organic absorption. Org. Geochem. 19 (1–3), 77–87. https://doi.org/10.1016/0146-6380(92)90028-V.

Sang, Q., Zhang, S.J., Li, Y.J., et al., 2018. Determination of organic and inorganic hydrocarbon saturations and effective porosities in shale using vacuum-imbibition method. Int. J. Coal Geol. 200, 123–134. https://doi.org/10.1016/j.coal.2018.10.010.

Scarlat, N., Dallemand, J.F., Monforti-Ferrario, F., et al., 2015. Renewable energy policy framework and bioenergy contribution in the European union—an overview from National renewable energy action plans and progress reports. Renew. Sustain. Energy Rev. 51, 969–985. https://doi.org/10.1016/j.rser.2015.06.062.

Schettler, P.D., Parmely, C.R., 1991. Contributions to total storage capacity in Devonian shales. SPE Eastern Regional Meeting. OnePetro. https://doi.org/10.2523/23422-ms.

Schmoker, J.W., 1996. A Resource Evaluation of the Bakken Formation (Upper Devonian and Lower Mississippian) Continuous Oil Accumulation, Williston Basin. In: The Mountain Geologist. North Dakota and Montana, p. 33.

Shao, X.H., Pang, X.Q., Li, H., et al., 2018. Pore network characteristics of lacustrine shales in the Dongpu Depression, Bohai Bay Basin, China, with implications for oil retention. Mar. Petrol. Geol. 96, 457–473. https://doi.org/10.1016/j.marpetgeo.2018.06.015.

Shou, J.F., Yuan, Z.W., 1990. Diagenesis and oil-gas relationship of sub member sha 3(3) of oligocene Shahejie Formation in Machang area, Dongpu depression. Oil & Gas Geology 11 (2), 187–194. https://doi.org/10.11743/ogg19900207.

Sing, K.S.W., 1985. Reporting physisorption data for gas/solid systems with special reference to the determination of surface area and porosity (Recommendations 1984). Pure Appl. Chem. 57 (4), 603–619. https://doi.org/10.1351/pac198557040603.

Snarsky, A.N., 1962. Die primare migration des erdols. Freiberger Forschungsch 123, 63–73.

Soeder, D.J., 2018. The successful development of gas and oil resources from shales in North America. J. Petrol. Sci. Eng. 163, 399–420. https://doi.org/10.1016/j.petrol.2017.12.084.

Song, Y., Li, S.F., Hu, S.Z., 2019. Warm-humid paleoclimate control of salinized lacustrine organic-rich shale deposition in the Oligocene Hetaoyuan Formation of the Biyang Depression, East China. Int. J. Coal Geol. 202, 69–84. https://doi.org/10.1016/j.coal.2018.11.016.

Song, D.J., Wang, X.Q., Wu, C.J., et al., 2020. Petroleum generation, retention, and expulsion in lacustrine shales using an artificial thermal maturation approach: implications for the in-situ conversion of shale oil. Energy Fuels 35 (1), 358–373. https://doi.org/10.1021/acs.energyfuels.0c03045.

Spigolon, A.L.D., Lewan, M.D., de Barros Penteado, H.L., et al., 2015. Evaluation of the petroleum composition and quality with increasing thermal maturity as simulated by hydrous pyrolysis: a case study using a Brazilian source rock with Type I kerogen. Org. Geochem. 83, 27–53. https://doi.org/10.1016/j.orggeochem.2015.03.001.

Su, H., Qu, L.P., Zhang, J.C., et al., 2006. Tectonic evolution and extensional pattern of rifted basin: a case study of Dongpu depression. Oil Gas Geol. 27 (1), 70–77. https://doi.org/10.11743/ogg20060112.

Su, S.Y., Jiang, Z.X., Shan, X.L., et al., 2019. Effect of lithofacies on shale reservoir and hydrocarbon bearing capacity in the Shahejie Formation, Zhanhua Sag, eastern China. J. Petrol. Sci. Eng. 174, 1303–1308. https://doi.org/10.1016/j.petrol.2018.11.048.

Sun, Y.C., 1996. Diagenesis of Petroliferous Faulted Basins in Eastern China. Science Press, Beijing.

Sweeney, J.J., Burnham, A.K., 1990. Evaluation of a simple model of vitrinite reflectance based on chemical kinetics. AAPG Bull. 74 (10), 1559–1570. https://doi.org/10.1306/0C9B251F-1710-11D7-8645000102C1865D.

Tan, F.Q., Ju, Y.W., Xu, H.W., 2015. Present situation and technical developing tendency of shale gas development in China. Acta Geol. Sin. 89 (1), 409–411. https://doi.org/10.1111/1755-6724.12307_1.

Tänavsuu-Milkeviciene, K., Frederick Sarg, J., 2012. Evolution of an organic-rich lake basin–stratigraphy, climate and tectonics: Piceance Creek basin, Eocene Green River Formation. Sedimentology 59 (6), 1735–1768. https://doi.org/10.1111/j.1365-3091.2012.01324.x.

Tang, X., Zhang, J.C., Wang, X.Z., et al., 2014. Shale characteristics in the southeastern Ordos Basin, China: implications for hydrocarbon accumulation conditions and the potential of continental shales. Int. J. Coal Geol. 128, 32–46. https://doi.org/10.1016/j.coal.2014.03.005.

Tang, X., Zhu, Y.M., Liu, Y., 2017. Investigation of shale nano-pore characteristics by scanning electron microscope and low-pressure nitrogen adsorption. J. Nanosci. Nanotechnol. 17 (9), 6252–6261. https://doi.org/10.1166/jnn.2017.14485.

Tang, X., Zhang, J.C., Wang, X.Z., et al., 2018. Heterogeneity of organic-rich lacustrine marlstone succession and their controls to petroleum expulsion, retention, and migration: a case study in the Shulu Sag, Bohai Bay Basin, China. Mar. Petrol. Geol. 96, 166–178. https://doi.org/10.1016/j.marpetgeo.2018.05.031.

Theuerkorn, K., Horsfield, B., Wilkes, H., et al., 2008. A reproducible and linear method for separating asphaltenes from crude oil. Org. Geochem. 39 (8), 929–934. https://doi.org/10.1016/j.orggeochem.2008.02.009.

Thommes, M., Kaneko, K., Neimark, A.V., et al., 2015. Physisorption of gases, with special reference to the evaluation of surface area and pore size distribution (IUPAC Technical Report). Pure Appl. Chem. 87 (9–10), 1051–1069. https://doi.org/10.1515/pac-2014-1117.

Thyberg, B., Jahren, J., Winje, T., et al., 2010. Quartz cementation in Late Cretaceous mudstones, northern North Sea: changes in rock properties due to dissolution of smectite and precipitation of micro-quartz crystals. Mar. Petrol. Geol. 27 (8), 1752–1764. https://doi.org/10.1016/j.marpetgeo.2009.07.005.

Tissot, P.B., Welte, D.H., 1984. Petroleum formation and occurrence. Springer-verlag 546–563.

Torgersen, T., De Deckker, P., Chivas, A.R., et al., 1986. Salt lakes: a discussion of processes influencing palaeoenvironmental interpretation and recommendations for future study. Palaeogeogr. Palaeoclimatol. Palaeoecol. 54 (1–4), 7–19. https://doi.org/10.1016/0031-0182(86)90115-X.

Valyashko, M.G., 1963. Genesis of the Brines of the Sedimentary Envelope. Chemistry of the Earth's Crust, vol. 1. Akademii Nauk, Moscow, pp. 263–290.

Vankreve, D.W., 1965. Chemical structure and properties of coal. 28. coal constitution and solvent extraction. Fuel 44 (4), 229.

Wang, X.L., Zhang, X.Y., Wang, Y.S., et al., 2002. Discussion on genesis of halites and petroleum accumulation in Dongpu Depression. Pet. Geol. Oilfield Dev. Daqing 21 (5), 11–12 (in Chinese).

Wang, M., Sherwood, N., Li, Z.S., et al., 2015. Shale oil occurring between salt intervals in the Dongpu depression, Bohai Bay Basin, China. Int. J. Coal Geol. 152, 100–112. https://doi.org/10.1016/j.coal.2015.07.004.

Wang, S., Javadpour, F., Feng, Q.H., 2016. Molecular dynamics simulations of oil transport through inorganic nanopores in shale. Fuel 171, 74–86. https://doi.org/10.1016/j.fuel.2015.12.071.

Wang, R.Y., Gong, D.J., Leng, J.G., et al., 2017. Developmental characteristics of the lower Cambrian Niutitang shale reservoir in Northern Guizhou area: a case study in the Cengong block. Earth Sci. Front. 24 (6), 286–299. https://doi.org/10.11743/ogg20160107.

Wang, Y.M., Wang, H.K., Zhang, C., et al., 2017. Fracture pore evaluation of the upper ordovician Wufeng to lower silurian longmaxi formations in southern Sichuan basin, SW China. Petrol. Explor. Dev. 44 (4), 563–572. https://doi.org/10.1016/S1876-3804(17)30065-4.

Wang, M., Guo, Z.Q., Jiao, C.X., et al., 2019a. Exploration progress and geochemical features of lacustrine shale oils in China. J. Petrol. Sci. Eng. 178, 975–986. https://doi.org/10.1016/j.petrol.2019.04.029.

Wang, Q.T., Wang, T.L., Liu, W.P., et al., 2019b. Relationships among composition, porosity and permeability of longmaxi shale reservoir in the Weiyuan block, Sichuan basin, China. Mar. Petrol. Geol. 102, 33–47. https://doi.org/10.1016/j.marpetgeo.2018.12.026.

Wang, M., Chen, H.H., Huang, C.J., et al., 2020a. Astronomical forcing and sedimentary noise modeling of lake-level changes in the Paleogene Dongpu Depression of North China. Earth Planet Sci. Lett. 116116, 535. https://doi.org/10.1016/j.epsl.2020.116116.

Wang, Q.F., Jiang, F.J., Ji, H.C., et al., 2020b. Differential enrichment of organic matter in saline lacustrine source rocks in a rift basin: a case study of Paleogene source rocks, Dongpu Depression, Bohai Bay Basin. Nat. Resour. Res. 29 (6), 4053–4072. https://doi.org/10.1007/s11053-020-09671-x.

Wang, Q.F., Jiang, F.J., Ji, H.C., et al., 2020c. Effects of paleosedimentary environment on organic matter enrichment in a saline lacustrine rift basin-A case study of Paleogene source rock in the Dongpu Depression, Bohai Bay Basin. J. Petrol. Sci. Eng. 107658, 195. https://doi.org/10.1016/j.petrol.2020.107658.

Wang, Y.X., Xu, S., Hao, F., et al., 2021. Arid climate disturbance and the development of salinized lacustrine oil shale in the Middle Jurassic Dameigou Formation, Qaidam Basin, northwestern China. Palaeogeography, Palaeoclimatology. Palaeoecology 110533, 577. https://doi.org/10.1016/j.palaeo.2021.110533.

Wang, E.Z., Feng, Y., Guo, T.L., et al., 2022a. Oil content and resource quality evaluation methods for lacustrine shale: a review and a novel three-dimensional quality evaluation model. Earth Sci. Rev. 104134. https://doi.org/10.1016/j.earscirev.2022.104134.

Wang, K., Ma, L., Taylor, K.G., 2022b. Nanoscale geochemical heterogeneity of organic matter in thermally-mature shales: an AFM-IR study. Fuel 122278, 310. https://doi.org/10.1016/j.fuel.2021.122278.

Wei, L., Mastalerz, M., Schimmelmann, A., et al., 2014. Influence of Soxhlet-extractable bitumen and oil on porosity in thermally maturing organic-rich shales. Int. J. Coal Geol. 132, 38–50. https://doi.org/10.1016/j.coal.2014.08.003.

Wilhelms, A., Larter, S.R., Leythaeuser, D., et al., 1990. Recognition and quantification of the effects of primary migration in a Jurassic clastic source-rock from the Norwegian continental shelf. Org. Geochem. 16 (1–3), 103–113. https://doi.org/10.1016/0146-6380(90)90030-4.

Wu, L.L., Geng, A.S., Wang, P., 2018. Oil expulsion in marine shale and its influence on the evolution of nanopores during semi-closed pyrolysis. Int. J. Coal Geol. 191, 125–134. https://doi.org/10.1016/j.coal.2018.04.001.

Wu, L.L., Wang, P., Geng, A.S., 2019. Later stage gas generation in shale gas systems based on pyrolysis in closed and semi-closed systems. Int. J. Coal Geol. 206, 80–90. https://doi.org/10.1016/j.coal.2019.03.011.

Xi, Z.D., Tang, S.H., Zhang, S.H., et al., 2019. Characterization of quartz in the Wufeng Formation in northwest Hunan Province, south China and its implications for reservoir quality. J. Petrol. Sci. Eng. 179, 979–996. https://doi.org/10.1016/j.petrol.2019.04.051.

Xue, Q.Z., Tao, Y.H., Liu, Z.L., et al., 2015. Mechanism of oil molecules transportation in nano-sized shale channel: MD simulation. RSC Adv. 5 (33), 25684–25692. https://doi.org/10.1039/C4RA16682E.

Yang, X.R., Yan, D.T., Wei, X.S., et al., 2018. Different formation mechanism of quartz in siliceous and argillaceous shales: a case study of Longmaxi Formation in South China. Mar. Petrol. Geol. 94, 80–94. https://doi.org/10.1016/j.marpetgeo.2018.03.036.

Yin, A., Harrison, T.M., 2000. Geologic evolution of the Himalayan-Tibetan orogen. Annu. Rev. Earth Planet Sci. 28 (1), 211–280. https://doi.org/10.1146/annurev.earth.28.1.211.

Yue, H.W., Vieth-Hillebrand, A., Han, Y.J., et al., 2021. Unravelling the impact of lithofacies on the composition of NSO compounds in residual and expelled fluids of the Barnett, Niobrara and Posidonia formations. Org. Geochem. 104225, 155. https://doi.org/10.1016/j.orggeochem.2021.104225.

Zhang, H.F., 1992. New Advanced in petroleum geology. Oil Gas Geol. 13, 351–354. https://doi.org/10.11743/ogg19920313.

Zhang, Z.H., Yang, F., 1998. Biomarker assemblage characteristics of source rocks and associated crude oils in saline lake facies of Cenozoic in China. Acta Sedimentol. Sin. 16, 119–123. https://doi.org/10.1088/0256-307X/16/9/027.

Zhang, J.G., Jiang, Z.X., Liang, C., et al., 2016. Lacustrine massive mudrock in the Eocene Jiyang depression, Bohai Bay Basin, China: nature, origin and significance. Mar. Petrol. Geol. 77, 1042–1055. https://doi.org/10.1016/j.marpetgeo.2016.08.008.

Zhang, Y.X., Hu, Q.H., Long, S.X., et al., 2019a. Mineral-controlled nm-μm-scale pore structure of saline lacustrine shale in Qianjiang Depression, Jianghan Basin, China. Mar. Petrol. Geol. 99, 347–354. https://doi.org/10.1016/j.marpetgeo.2018.10.016.

Zhang, Y.H., Wang, Y.F., Ma, W., et al., 2019b. Compositional characterization of expelled and residual oils in the source rocks from oil generation–expulsion thermal simulation experiments. ACS Omega 4 (5), 8239–8248. https://doi.org/10.1021/acsomega.9b00260.

Zhang, J.N., Zhou, J.S., Fu, L.X., et al., 2020. Karstification of Ordovician carbonate reservoirs in Huanghua depression and its control factors. Carbonates Evaporites 35 (2), 1–16. https://doi.org/10.1007/s13146-020-00572-x.

Zhang, P.Y., Jiang, F.J., Zhu, C.X., et al., 2021a. Gas generation potential and characteristics of oil-prone shale in the saline lacustrine rifting basins: a case study of the Dongpu Depression, Bohai Bay Basin. Energy Fuels 35 (3), 2192–2208. https://doi.org/10.1021/acs.energyfuels.0c03965.

Zhang, P.L., Misch, D., Meng, Q.T., et al., 2021b. Comprehensive thermal maturity assessment in shales: a case study on the upper cretaceous Qingshankou formation (Songliao Basin, NE China). Int. J. Earth Sci. 110 (3), 943–962. https://doi.org/10.1007/s00531-021-02000-4.

Zhang, P.Y., Wang, Y.L., Zhang, X.J., et al., 2022. Carbon, oxygen and strontium isotopic and elemental characteristics of the Cambrian Longwangmiao Formation in South China: paleoenvironmental significance and implications for carbon isotope excursions. Gondwana Res. 106, 174–190. https://doi.org/10.1016/j.gr.2022.01.008.

Zhao, C.L., Liu, M.H., Ji, Y.L., 1992. Sedimentary System and Diagenesis of Eogene Clastic Rocks in Dongpu Depression. Petroleum Industry Press.

Zheng, R.C., Yang, M.Q., 1999. Study on paleosalinity of Chang 6 Formation in Ordos basin. Oil Gas Geol. 20, 20–25. https://doi.org/10.11743/ogg19990105 (in Chinese).

Zhu, W.Y., Reinfelder, J.R., 2012. The microbial community of a black shale pyrite biofilm and its implications for pyrite weathering. Geomicrobiol. J. 29 (2), 186–193. https://doi.org/10.1080/01490451.2010.539663.

Zhu, Y.M., Weng, H.X., Su, A.G., et al., 2006. Geochemical characteristics of Tertiary saline lacustrine oils in the Western Qaidam Basin, northwest China. Appl. Geochem. 20 (10), 1875–1889. https://doi.org/10.1016/j.apgeochem.2005.06.003.

Zhu, R.F., Zhang, L.Y., Li, J.Y., et al., 2015. Quantitative evaluation of residual liquid hydrocarbons in shale. Acta Pet. Sin. 36, 13–18. https://doi.org/10.7623/syxb201501002 (in Chinese).

Zhu, C.X., Jiang, F.J., Zhang, P.Y., et al., 2021. Identification of effective source rocks in different sedimentary environments and evaluation of hydrocarbon resources potential: a case study of paleogene source rocks in the Dongpu Depression, Bohai Bay Basin. J. Petrol. Sci. Eng. 108477, 201. https://doi.org/10.1016/j.petrol.2021.108477.

Zou, Y.R., Shuai, Y.H., Kong, F., et al., 2004. Experiments on petroleum generation–Considerations and outlook. Petrol. Geol. Exp. 26, 375–382. https://doi.org/10.11781/sysydz200404375.

Zou, C.N., Tao, S.Z., Yang, Z., et al., 2012. New advanced in unconventional petroleum exploration and research in China. Bulletin of Mineralogy. Petrol. Geochem. 31, 312–322. https://doi.org/10.3969/j.issn.1007-2802.2012.04.002 (in Chinese).

Zou, C.N., Pan, S.Q., Horsfield, B., et al., 2019a. Oil retention and intrasource migration in the organic-rich lacustrine Chang 7 shale of the upper Triassic Yanchang formation, Ordos basin, central China. AAPG (Am. Assoc. Pet. Geol.) Bull. 103 (11), 2627–2663x. https://doi.org/10.1306/01301917052.

Zou, C.N., Zhu, R.K., Chen, Z.Q., et al., 2019b. Organic-matter-rich shales of China. Earth Sci. Rev. 189, 51–78. https://doi.org/10.1016/j.earscirev.2018.12.002.